of ethanol was added 0.2 mL of NaOMe (28% in methanol). The reaction mixture was stirred for 12 h at room temperature. The precipitate was collected by filtration, washed with water and hexane, and recrystallized from ethanol. Yield, 88.3%. ^{1}H NMR (400 MHz, $CDCL_3$): δ 7.81 (s, 2H), 7.51−7.31 (m, 12H), 2.94 (dd, J = 8.3, 3.9 Hz, 4H), 1.80 (dt, J = 12.3, 6.3 Hz, 2H). MS (ESI): m/z calcd for $C_{20}H_{18}O$, 274.14; found, 275.10 ($M + H^+$).

*(2E,6E)-2,6-Bis(4-chlorobenzylidene)cyclohexanone (**62**).* The same reaction described above to prepare **61** was used. Compound **62** was obtained in a yield of 71.2%. ^{1}H NMR (400 MHz, $CDCL_3$): δ 7.73 (s, 2H), 7.38 (s, 8H), 2.89 (dd, J = 8.3, 3.9 Hz, 4H), 1.81 (dd, J = 12.0, 6.0 Hz, 2H). MS (ESI): m/z calcd for $C_{20}H_{16}Cl_2O$, 342.06; found, 343.10 ($M + H^+$).

*(2E,6E)-2,6-Bis(4-methoxybenzylidene)cyclohexanone (**63**).* The same reaction described above to prepare **61** was used, and **63** was obtained in a yield of 74.3%. ^{1}H NMR (400 MHz, $CDCL_3$): δ 7.76 (s, 2H), 7.45 (d, J = 8.8 Hz, 4H), 6.94 (d, J = 8.8 Hz, 4H), 3.84 (s, 6H), 3.05−2.84 (m, 4H), 1.81 (dd, J = 11.9, 5.8 Hz, 2H). MS (ESI): m/z calcd for $C_{22}H_{22}O_3$, 334.16; found, 335.05 ($M + H^+$).

*(2E,6E)-2,6-Bis(4-(dimethylamino)benzylidene)cyclohexanone (**64**).* The same reaction described above to prepare **61** was used, and **64** was obtained in a yield of 12.3%. ^{1}H NMR (400 MHz, $CDCL_3$): δ 7.75 (s, 2H), 7.44 (d, J = 8.9 Hz, 4H), 6.71 (d, J = 8.9 Hz, 4H), 3.01 (s, 12H), 2.96−2.90 (m, 4H), 1.82 (dd, J = 11.8, 5.7 Hz, 2H). MS (ESI): m/z calcd for $C_{24}H_{28}N_2O$, 360.22; found, 361.15 ($M + H^+$).

*(E)-4-(4-Nitrophenyl)but-3-en-2-one (**65**).* To a solution of 4-nitrobenzaldehyde (6.04 g, 50 mmol) in 150 mL of acetone were added 1.38 g of K_2CO_3 and 10 mL of water, and the reaction mixture was stirred for 12 h at room temperature. Then, 20 mL of concentrated HCl was added, and the mixture was stirred for an additional 6 h at room temperature. After 300 mL of water was added, the white precipitate formed was collected by filtration, washed with water, and dried under vacuum to obtain 8.34 g of **65** (87.2%). ^{1}H NMR (400 MHz, $CDCL_3$): δ 8.26 (d, J = 8.9 Hz, 2H), 7.70 (d, J = 8.8 Hz, 2H), 7.54 (d, J = 16.3 Hz, 1H), 6.82 (d, J = 16.3 Hz, 1H), 2.42 (s, 3H). MS (ESI): m/z calcd for $C_{10}H_9NO_3$, 191.06; found, 192.10 ($M + H^+$).

*(E)-4-(4-Aminophenyl)but-3-en-2-one (**66**).* A mixture of **65** (1.92 g, 10 mmol) and $SnCl_2$ (3.79 g, 20 mmol) dissolved in 80 mL of ethanol containing 5 mL of concentrated hydrochloric acid was stirred under reflux for 2 h. After the mixture was cooled to room temperature, 2 M NaOH (100 mL) was added and extracted with ethyl acetate (100 mL). The organic layer was dried over Na_2SO_4. The solvent was removed, and the residue was purified by silica gel chromatography to give 1.16 g of **66** (72.1%). ^{1}H NMR (400 MHz, $CDCL_3$): δ 7.44 (d, J = 16.2 Hz, 1H), 7.37 (d, J = 8.7 Hz, 2H), 6.66 (d, J = 8.6 Hz, 2H), 6.55 (d, J = 16.1 Hz, 1H), 4.00 (s, 2H), 2.34 (s, 3H). MS (ESI): m/z calcd for $C_{10}H_{11}NO$, 161.08; found, 162.10 ($M + H^+$).

*(E)-4-(4-(Methylamino)phenyl)but-3-en-2-one (**67**).* To a solution of **66** (483 mg, 3 mmol) and 414 mg of K_2CO_3 in 50 mL of acetone was added CH_3I (852 mg, 6 mmol) dropwise, and the reaction mixture was stirred for 8 h at room temperature. After filtration, the solvent was removed, and the residue was purified by silica gel chromatography to give 183.5 mg of **67** (34.9%). ^{1}H NMR (400 MHz, $CDCL_3$): δ 7.45 (d, J = 16.1 Hz, 1H), 7.40 (d, J = 8.7 Hz, 2H), 6.58 (d, J = 8.7 Hz, 2H), 6.54 (d, J = 16.1 Hz, 1H), 4.13 (s, 1H), 2.88 (s, 3H), 2.33 (s, 3H). MS (ESI): m/z calcd for $C_{11}H_{13}NO$, 175.10; found, 176.15 ($M + H^+$).

*(1E,4E)-1-(4-Aminophenyl)-5-(4-bromophenyl)penta-1,4-dien-3-one (**68**).* Compound **68** was prepared following general procedure A. Yield, 55.7%. ^{1}H NMR (400 MHz, $CDCL_3$): δ 7.68 (d, J = 15.8 Hz, 1H), 7.63 (d, J = 15.9 Hz, 1H), 7.54 (d, J = 8.5 Hz, 2H), 7.46 (d, J = 8.5 Hz, 2H), 7.45 (d, J = 8.5 Hz, 2H), 7.05 (d, J = 15.9 Hz, 1H), 6.87 (d, J = 15.8 Hz, 1H), 6.68 (d, J = 8.6 Hz, 2H), 4.01 (s, 1H). MS (ESI): m/z calcd for $C_{17}H_{14}BrNO$, 327.03; found, 328.05 ($M + H^+$).

*(1E,4E)-1-(4-Bromophenyl)-5-(4-(methylamino)phenyl)penta-1,4-dien-3-one (**69**).* Compound **69** was prepared following general procedure A. Yield, 63.1%. ^{1}H NMR (400 MHz, $CDCL_3$): δ 7.70 (d, J = 15.8 Hz, 1H), 7.62 (d, J = 15.9 Hz, 1H), 7.53 (d, J = 8.5 Hz, 2H), 7.48 (d, J = 8.3 Hz, 2H), 7.46 (d, J = 8.5 Hz, 2H), 7.06 (d, J = 15.9 Hz, 1H), 6.85 (d, J = 15.7 Hz, 1H), 6.59 (d, J = 8.6 Hz, 2H), 2.90 (s, 3H). MS (ESI): m/z calcd for $C_{18}H_{16}BrNO$, 341.04; found, 342.10 ($M + H^+$).

*(1E,4E)-1-(4-Aminophenyl)-5-(4-iodophenyl)penta-1,4-dien-3-one (**70**).* Compound **70** was prepared following general procedure A. Yield, 46.1%. ^{1}H NMR (400 MHz, $CDCL_3$): δ 7.74 (d, J = 8.4 Hz, 2H), 7.68 (d, J = 15.8 Hz, 1H), 7.61 (d, J = 15.9 Hz, 1H), 7.45 (d, J = 8.5 Hz, 2H), 7.33 (d, J = 8.4 Hz, 2H), 7.06 (d, J = 15.9 Hz, 1H), 6.87 (d, J = 15.8 Hz, 1H), 6.68 (d, J = 8.5 Hz, 2H), 4.01 (s, 2H). HRMS (EI): m/z (EI^+): calcd for $C_{17}H_{14}INO$, 375.0120; found, 375.0116.

*(1E,4E)-1-(4-Iodophenyl)-5-(4-(methylamino)phenyl)penta-1,4-dien-3-one (**71**).* Compound **71** was prepared following general procedure A. Yield, 53.2%. ^{1}H NMR (400 MHz, $CDCL_3$): δ 7.74 (d, J = 8.4 Hz, 2H), 7.70 (d, J = 15.8 Hz, 1H), 7.61 (d, J = 15.8 Hz, 1H), 7.48 (d, J = 8.7 Hz, 2H), 7.33 (d, J = 8.5 Hz, 2H), 7.07 (d, J = 15.9 Hz, 1H), 6.85 (d, J = 15.8 Hz, 1H), 6.60 (d, J = 8.7 Hz, 2H), 4.18 (s, 1H), 2.90 (s, 3H). HRMS (EI): m/z (EI^+): calcd for $C_{18}H_{16}INO$, 389.0277; found, 389.0281.

*(1E,4E)-1-(4-Aminophenyl)-5-(4-(tributylstannyl)phenyl)penta-1,4-dien-3-one (**72**).* A mixture of **68** (125 mg, 0.38 mmol), $(Bu_3Sn)_2$ (440.9 mg, 0.76 mmol), and $(Ph_3P)_4Pd$ (47 mg, 0.04 mmol) in toluene (10 mL) was stirred under reflux for 10 h. The solvent was removed, and the residue was purified by silica gel chromatography to give 46.8 mg of **72** (22.9%). ^{1}H NMR (400 MHz, $CDCL_3$): δ 7.69 (d, J = 15.9 Hz, 1H), 7.68 (d, J = 15.8 Hz, 1H), 7.54 (d, J = 8.4 Hz, 2H), 7.51 (d, J = 8.1 Hz, 2H), 7.45 (d, J = 8.5 Hz, 2H), 7.08 (d, J = 15.9 Hz, 1H), 6.90 (d, J = 15.8 Hz, 1H), 6.67 (d, J = 8.5 Hz, 2H), 4.00 (s, 1H), 1.71−0.71 (m, 27H). MS (ESI): m/z calcd for $C_{29}H_{41}NOSn$, 539.22; found, 540.30 ($M + H^+$).

*(1E,4E)-1-(4-(Methylamino)phenyl)-5-(4-(tributylstannyl)phenyl) penta-1,4-dien-3-one (**73**).* The same reaction described above to prepare **72** was used. Compound **73** was obtained in a yield of 30.2%. ^{1}H NMR (400 MHz, $CDCL_3$): δ 7.69 (d, J = 15.8 Hz, 1H), 7.69 (d, J = 15.9 Hz, 1H), 7.54 (d, J = 8.0 Hz, 2H), 7.53 (d, J = 8.0 Hz, 2H), 7.48 (d, J = 8.6 Hz, 2H), 7.09 (d, J = 15.9 Hz, 1H), 6.88 (d, J = 15.7 Hz, 1H), 6.60 (d, J = 8.4 Hz, 2H), 4.12 (s, 1H), 2.90 (s, 3H), 1.82−0.58 (m, 27H). MS (ESI): m/z calcd for $C_{30}H_{43}NOSn$, 552.24; found, 553.25 ($M + H^+$).

*(1E,4E)-1-(4-(Dimethylamino)phenyl)-5-(4-(tributylstannyl)phenyl) penta-1,4-dien-3-one (**74**).* The reaction described above to prepare **72** was used, and **74** was obtained in a yield of 26.9%. ^{1}H NMR (400 MHz, $CDCL_3$): δ 7.71 (d, J = 15.7 Hz, 1H), 7.69 (d, J = 15.9 Hz, 1H), 7.60−7.44 (m, 6H), 7.10 (d, J = 15.9 Hz, 1H), 6.88 (d, J = 15.8 Hz, 1H), 6.69 (d, J = 8.9 Hz, 2H), 3.03 (s, 6H), 1.82−0.77 (m, 27H). MS (ESI): m/z calcd for $C_{31}H_{45}$, 567.25; found, 568.25 ($M + H^+$).

*(1E,4E)-1-(4-(Dimethylamino)phenyl)-5-(4-(2-hydroxyethoxy)phenyl) penta-1,4-dien-3-one (**75**).* Compound **75** was prepared following general procedure A. Yield, 89.8%. ^{1}H NMR (400 MHz, $CDCL_3$): δ 7.71 (d, J = 15.5 Hz, 1H), 7.68 (d, J = 15.8 Hz, 1H), 7.57 (d, J = 8.1 Hz, 2H), 7.52 (d, J = 8.2 Hz, 2H), 6.98 (d, J = 16.0 Hz, 1H), 6.95 (d, J = 8.0 Hz, 2H), 6.88 (d, J = 15.8 Hz, 1H), 6.70 (d, J = 8.2 Hz, 2H), 4.14 (t, J = 4.0 Hz, 2H), 4.05−3.92 (m, 2H), 3.05 (s, 6H). MS (ESI): m/z calcd for $C_{21}H_{23}NO_3$, 337.17; found, 338.10 ($M + H^+$).

*(1E,4E)-1-(4-(Dimethylamino)phenyl)-5-(4-(2-(2-hydroxyethoxy)-ethoxy)phenyl)penta-1,4-dien-3-one (**76**).* Compound **76** was prepared following general procedure A. Yield, 84.3%. ^{1}H NMR (400 MHz, $CDCL_3$): δ 7.70 (d, J = 15.8 Hz, 1H), 7.67 (d, J = 15.8 Hz, 1H), 7.56 (d, J = 8.8 Hz, 2H), 7.52 (d, J = 8.9 Hz, 2H), 6.97 (d, J = 15.2 Hz, 1H), 6.94 (d, J = 8.6 Hz, 2H), 6.87 (d, J = 15.8 Hz, 1H), 6.70 (d, J = 8.8 Hz, 2H), 4.29−4.11 (m, 2H), 3.96−3.84 (m, 2H), 3.80−3.75 (m, 2H), 3.72−3.65 (m, 2H), 3.04 (s, 6H). MS (ESI): m/z calcd for $C_{23}H_{27}NO_4$, 381.19; found, 382.10 ($M + H^+$).

*(1E,4E)-1-(4-(Dimethylamino)phenyl)-5-(4-(2-(2-(2-hydroxyethoxy)ethoxy)ethoxy)phenyl)penta-1,4-dien-3-one (**77**).* Compound **77** was prepared following general procedure A. Yield, 79.2%. ^{1}H NMR

(400 MHz, $CDCl_3$): δ 7.70 (d, J = 12.0 Hz, 1H), 7.67 (d, J = 12.1 Hz, 1H), 7.55 (d, J = 8.8 Hz, 2H), 7.52 (d, J = 8.9 Hz, 2H), 6.97 (d, J = 13.9 Hz, 2H), 6.94 (d, J = 6.8 Hz, 1H), 6.87 (d, J = 15.7 Hz, 1H), 6.69 (d, J = 8.9 Hz, 2H), 4.19−4.16 (m, 2H), 3.91−3.85 (m, 2H), 3.77−3.68 (m, 6H), 3.66−3.59 (m, 2H), 3.04 (s, 6H). MS (ESI): m/z calcd for $C_{25}H_{31}NO_5$, 425.22; found, 426.25 ($M + H^+$).

*2-(4-((1E,4E)-5-(4-(Dimethylamino)phenyl)-3-oxopenta-1,4-dien-1-yl)-phenoxy)ethyl 4-methylbenzenesulfonate (**78**).* To a solution of **75** (101 mg, 0.3 mmol) in pyridine (8 mL) was added tosyl chloride (69 mg, 0.36 mmol). The reaction mixture was stirred for 3 h at room temperature, 50 mL of water was added, and the mixture was extracted with $CHCl_3$. The organic layer was dried over Na_2SO_4, and evaporation of the solvent afforded a residue, which was purified by silica gel chromatography to give 69.2 mg of **78** (46.9%). ^{1}H NMR (400 MHz, $CDCL_3$): δ 7.82 (d, J = 8.3 Hz, 2H), 7.70 (d, J = 15.8 Hz, 1H), 7.65 (d, J = 15.9 Hz, 1H), 7.52 (d, J = 8.8 Hz, 2H), 7.52 (d, J = 9.0 Hz, 2H), 6.97 (d, J = 15.8 Hz, 1H), 6.86 (d, J = 15.7 Hz, 1H), 6.80 (d, J = 8.8 Hz, 2H), 6.70 (d, J = 8.9 Hz, 2H), 4.50−4.32 (m, 2H), 4.19 (dd, J = 5.5, 3.9 Hz, 2H), 3.04 (s, 6H), 2.45 (s, 3H). MS (ESI): m/z calcd for $C_{28}H_{29}NO_5S$, 491.18; found, 492.34 ($M + H^+$).

*2-(2-(4-((1E,4E)-5-(4-(Dimethylamino)phenyl)-3-oxopenta-1,4-dien-1-yl)phenoxy)ethoxy)ethyl 4-Methylbenzenesulfonate (**79**).* The same reaction described above to prepare **78** was used. Compound **79** was obtained in a yield of 37.5%. ^{1}H NMR (400 MHz, $CDCL_3$): δ 7.80 (d, J = 8.3 Hz, 2H), 7.70 (d, J = 15.7 Hz, 1H), 7.67 (d, J = 15.7 Hz, 1H), 7.55 (d, J = 8.7 Hz, 2H), 7.52 (d, J = 8.9 Hz, 2H), 7.30 (d, J = 8.4 Hz, 2H), 6.98 (d, J = 15.8 Hz, 1H), 6.91 (d, J = 8.8 Hz, 2H), 6.87 (d, J = 15.8 Hz, 1H), 6.70 (d, J = 8.9 Hz, 2H), 4.23−4.16 (m, 2H), 4.14−4.02 (m, 2H), 3.90−3.66 (m, 4H), 3.04 (s, 6H), 2.41 (s, 3H). MS (ESI): m/z calcd for $C_{30}H_{33}NO_6S$, 535.20; found, 536.17 ($M + H^+$).

*2-(2-(2-(4-((1E,4E)-5-(4-(Dimethylamino)phenyl)-3-oxopenta-1,4-dien-1-yl)phenoxy)ethoxy)ethoxy)ethyl 4-Methylbenzenesulfonate (**80**).* The reaction described above to prepare **78** was used, and **80** was obtained in a yield of 58.8%. ^{1}H NMR (400 MHz, $CDCL_3$): δ 7.80 (d, J = 8.2 Hz, 2H), 7.70 (d, J = 15.7 Hz, 1H), 7.67 (d, J = 15.8 Hz, 1H), 7.55 (d, J = 8.7 Hz, 2H), 7.52 (d, J = 8.8 Hz, 2H), 7.33 (d, J = 8.1 Hz, 2H), 6.97 (d, J = 15.9 Hz, 1H), 6.93 (d, J = 8.7 Hz, 2H), 6.87 (d, J = 15.7 Hz, 1H), 6.70 (d, J = 8.8 Hz, 2H), 4.16 (dd, J = 8.9, 4.0 Hz, 2H), 3.90−3.80 (m, 2H), 3.73−3.68 (m, 2H), 3.64 (ddd, J = 9.0, 5.6, 3.5 Hz, 4H), 3.04 (s, 6H), 2.43 (s, 3H). MS (ESI): m/z calcd for $C_{32}H_{37}NO_7S$, 579.23; found, 580.39 ($M + H^+$).

*(1E,4E)-1-(4-(Dimethylamino)phenyl)-5-(4-(2-fluoroethoxy)phenyl)-penta-1,4-dien-3-one (**81**).* To a solution of **78** (100 mg, 0.2 mmol) in 15 mL of dry tetrahydrofuran (THF) was added anhydrous TBAF (400 μL, 1 M in THF). The reaction mixture was refluxed for 3 h. After removal of the THF, the residue was purified by silica gel chromatography to give 33.9 mg of **81** (50.0%). ^{1}H NMR (400 MHz, $CDCL_3$): δ 7.71 (d, J = 15.7 Hz, 1H), 7.68 (d, J = 15.7 Hz, 1H), 7.57 (d, J = 8.8 Hz, 2H), 7.52 (d, J = 8.9 Hz, 2H), 6.98 (d, J = 15.1 Hz, 1H), 6.95 (d, J = 8.6 Hz, 2H), 6.87 (d, J = 15.7 Hz, 1H), 6.70 (d, J = 8.8 Hz, 2H), 5.09−4.58 (m, 2H), 4.27 (dd, J = 27.6, 4.2 Hz, 2H), 3.04 (s, 6H). MS (ESI): m/z calcd for $C_{21}H_{22}FNO_2$, 339.16; found, 340.17 ($M + H^+$).

*(1E,4E)-1-(4-(Dimethylamino)phenyl)-5-(4-(2-(2-fluoroethoxy)-ethoxy)phenyl)penta-1,4-dien-3-one (**82**).* The same reaction described above to prepare **81** was used. Compound **82** was obtained in a yield of 41.3%. ^{1}H NMR (400 MHz, $CDCL_3$): δ 7.70 (d, J = 15.7 Hz, 1H), 7.67 (d, J = 15.8 Hz, 1H), 7.56 (d, J = 8.7 Hz, 2H), 7.52 (d, J = 8.9 Hz, 2H), 6.97 (d, J = 14.9 Hz, 1H), 6.95 (d, J = 8.6 Hz, 2H), 6.87 (d, J = 15.7 Hz, 1H), 6.70 (d, J = 8.9 Hz, 2H), 4.67−4.53 (m, 1H), 4.28−4.11 (m, 2H), 4.02−3.75 (m, 4H), 3.66 (t, J = 5.9 Hz, 1H), 3.04 (s, 6H). MS (ESI): m/z calcd for $C_{23}H_{26}FNO_3$, 383.19; found, 384.21 ($M + H^+$).

*(1E,4E)-1-(4-(Dimethylamino)phenyl)-5-(4-(2-(2-(2-fluoroethoxy)-ethoxy)ethoxy)phenyl)penta-1,4-dien-3-one (**83**).* The reaction described above to prepare **81** was used, and **83** was obtained in a yield of 36.6%. ^{1}H NMR (400 MHz, $CDCL_3$): δ 7.70 (d, J = 15.5 Hz, 1H), 7.67 (d, J = 15.5 Hz, 1H), 7.55 (d, J = 7.2 Hz, 2H), 7.51 (d, J = 7.7 Hz, 2H), 6.97 (d, J = 16.0 Hz, 1H), 6.93 (d, J = 8.8 Hz, 2H), 6.86 (d, J = 15.7 Hz, 1H), 6.68 (d, J = 7.7 Hz, 2H), 4.67−4.59 (m, 1H), 4.53−4.45 (m, 1H), 4.17 (t, J = 3.9 Hz, 2H), 3.88 (t, J = 3.9 Hz, 2H), 3.83−3.77 (m, 1H), 3.77−3.67 (m, 5H), 3.03 (s, 6H). HRMS (EI): m/z (EI^+): calcd for $C_{25}H_{30}FNO_4$, 427.2159; found, 427.2152.

*4-(2-(2-(2-Fluoroethoxy)ethoxy)ethoxy)benzaldehyde (**84**).* To a solution of 4-(2-(2-(2-hydroxyethoxy)ethoxy)ethoxy)benzaldehyde (508 mg, 2 mmol) in $CHCl_3$ (5 mL) was added DAST (645 mg, 4 mmol) in a dry ice−acetone bath. The reaction mixture was stirred for 2 h at room temperature and then poured into a saturated $NaHSO_3$ solution and extracted with chloroform. The organic phase was separated, dried over $MgSO_4$, and filtered, and the residue was purified by silica gel chromatography to give 299 mg of **84** (58.3%). ^{1}H NMR (400 MHz, $CDCL_3$): δ 9.88 (s, 1H), 7.83 (d, J = 8.9 Hz, 2H), 7.02 (d, J = 8.8 Hz, 2H), 4.62 (dd, J = 4.6, 3.7 Hz, 1H), 4.50 (dd, J = 4.7, 3.7 Hz, 1H), 4.22 (dd, J = 5.4, 4.2 Hz, 2H), 3.90 (dd, J = 5.4, 4.2 Hz, 2H), 3.83−3.67 (m, 6H). MS (ESI): m/z calcd for $C_{13}H_{17}FO_4$, 256.11; found, 257.10 ($M + H^+$).

*(1E,4E)-1-(4-(2-(2-(2-Fluoroethoxy)ethoxy)ethoxy)phenyl)-5-(4-(methylamino)phenyl)penta-1,4-dien-3-one (**85**).* Compound **85** was prepared following general procedure A. Yield, 67.2%. ^{1}H NMR (400 MHz, $CDCL_3$): δ 7.68 (d, J = 15.8 Hz, 1H), 7.67 (d, J = 15.8 Hz, 1H), 7.54 (d, J = 8.8 Hz, 2H), 7.47 (d, J = 8.7 Hz, 2H), 6.96 (d, J = 15.8 Hz, 1H), 6.93 (d, J = 8.8 Hz, 2H), 6.86 (d, J = 15.8 Hz, 1H), 6.58 (d, J = 8.7 Hz, 2H), 4.62 (dd, J = 4.7, 3.7 Hz, 1H), 4.50 (dd, J = 4.7, 3.7 Hz, 1H), 4.26−4.11 (m, 2H), 3.88 (dd, J = 5.4, 4.2 Hz, 2H), 3.83−3.66 (m, 6H), 2.87 (s, 3H). HRMS (EI): m/z (EI^+): calcd for $C_{24}H_{28}FNO_4$, 413.2002; found, 413.2007.

*(1E,4E)-1-(4-(2-(2-(2-Hydroxyethoxy)ethoxy)ethoxy)phenyl)-5-(4-(methylamino)phenyl)penta-1,4-dien-3-one (**86**).* Compound **86** was prepared following general procedure A. Yield, 70.5%. ^{1}H NMR (400 MHz, $CDCL_3$): δ 7.68 (d, J = 15.8 Hz, 1H), 7.66 (d, J = 15.8 Hz, 1H), 7.54 (d, J = 8.8 Hz, 2H), 7.47 (d, J = 8.7 Hz, 2H), 6.95 (d, J = 15.8 Hz, 1H), 6.93 (d, J = 8.8 Hz, 2H), 6.85 (d, J = 15.7 Hz, 1H), 6.58 (d, J = 8.7 Hz, 2H), 4.20−4.13 (m, 2H), 3.93−3.83 (m, 2H), 3.72 (ddd, J = 5.8, 4.6, 2.8 Hz, 6H), 3.65−3.58 (m, 2H), 2.88 (s, 3H). MS (ESI): m/z calcd for $C_{24}H_{29}NO_5$, 411.20; found, 412.40 ($M + H^+$).

*(1E,4E)-1-(4-(Methylamino)phenyl)-5-(4-((2,2,3,3-tetramethyl-4,7,10-trioxa-3-siladodecan-12-yl)oxy)phenyl)penta-1,4-dien-3-one (**87**).* Compound **86** (659 mg, 1.60 mmol) and TBDMSCl (386 mg, 2.56 mmol) were dissolved in dichloromethane (15 mL) followed by imidazole (120 mg, 3.20 mmol). The solution was stirred at room temperature for 2 h. A white solid formed and was filtered off. After the filtrate was evaporated, the residue was purified by silica gel column chromatography to afford **87** (502 mg, 59.5%). ^{1}H NMR (400 MHz, $CDCL_3$): δ 7.61 (d, J = 15.7 Hz, 1H), 7.59 (d, J = 15.8 Hz, 1H), 7.44 (d, J = 8.7 Hz, 2H), 7.36 (d, J = 8.6 Hz, 2H), 6.88 (d, J = 15.9 Hz, 1H), 6.84 (d, J = 8.7 Hz, 2H), 6.77 (d, J = 15.7 Hz, 1H), 6.48 (d, J = 8.6 Hz, 2H), 4.46 (s, 1H), 4.05 (t, J = 5.3 Hz, 2H), 3.77 (t, J = 5.3 Hz, 2H), 3.70 (t, J = 5.3 Hz, 2H), 3.68−3.57 (m, 4H), 3.49 (t, J = 5.3 Hz, 2H), 2.74 (s, 3H), 0.83 (s, 9H). MS (ESI): m/z calcd for $C_{30}H_{43}NO_5Si$, 525.29; found, 526.29 ($M + H^+$).

*tert-Butylmethyl(4-((1E,4E)-3-oxo-5-(4-((2,2,3,3-tetramethyl-4,7,10-trioxa-3-siladodecan-12-yl)oxy)phenyl)penta-1,4-dien-1-yl)phenyl)-carbamate (**88**).* Under a nitrogen atmosphere, **87** (491 mg, 0.94 mmol) was dissolved in anhydrous THF (20 mL) followed by Boc-anhydride (408 mg, 1.87 mmol). The solution was refluxed for 48 h. After the reaction was complete, the solvent was removed, and the residue was purified by silica gel column chromatography to afford **88** (433 mg, 74.1%). ^{1}H NMR (400 MHz, $CDCL_3$): δ 7.64 (d, J = 15.9 Hz, 1H), 7.63 (d, J = 15.9 Hz, 1H), 7.51 (d, J = 3.6 Hz, 2H), 7.49 (d, J = 3.9 Hz, 2H), 7.24 (d, J = 8.6 Hz, 2H), 6.95 (d, J = 15.9 Hz, 1H), 6.89

(d, J = 16.0 Hz, 1H), 6.87 (s, J = 8.5 Hz, 2H), 4.17–4.06 (m, 2H), 3.84–3.80 (m, 2H), 3.71 (t, J = 5.4 Hz, 2H), 3.64 (qdd, J = 4.8, 3.7, 1.8 Hz, 4H), 3.51 (t, J = 5.4 Hz, 2H), 3.23 (s, 3H), 1.41 (s, 9H), 0.83 (s, 9H). MS (ESI): m/z calcd for $C_{35}H_{51}NO_7Si$, 625.34; found, 626.30 ($M + H^+$).

*tert-Butyl(4-((1E,4E)-5-(4-(2-(2-(2-hydroxyethoxy)ethoxy)ethoxy)-phenyl)-3-oxopenta-1,4-dien-1-yl)phenyl)(methyl)carbamate (**89**).* To a solution of **88** (433 mg, 0.69 mmol) in dry THF (15 mL) was added anhydrous TBAF (1.4 mL, 1 M in THF). The solution was stirred at room temperature for 2 h. After removal of the THF, the residue was purified by silica gel chromatography to give 300 mg of **89** (85.0%). ^{1}H NMR (400 MHz, $CDCL_3$): δ 7.70 (d, J = 15.9 Hz, 1H), 7.69 (d, J = 15.9 Hz, 1H), 7.57 (d, J = 5.2 Hz, 2H), 7.55 (d, J = 5.3 Hz, 2H), 7.31 (d, J = 8.4 Hz, 2H), 7.02 (d, J = 15.9 Hz, 1H), 6.96 (d, J = 16.3 Hz, 1H), 6.95 (d, J = 8.3 Hz, 2H), 4.21–4.14 (m, 2H), 3.92–3.84 (m, 2H), 3.76–3.66 (m, 6H), 3.65–3.58 (m, 2H), 3.29 (s, 3H), 1.48 (s, 9H). MS (ESI): m/z calcd for $C_{29}H_{37}NO_7$, 511.26; found, 534.35 ($M + Na^+$).

*2-(2-(2-(4-((1E,4E)-5-(4-((tert-Butoxycarbonyl)(methyl)amino)phenyl) -3-oxopenta-1,4-dien-1-yl)phenoxy)ethoxy)ethoxy)ethyl methanesulfonate (**90**).* Compound **89** (290 mg, 0.567 mmol) was dissolved in dichloromethane (15 mL) followed by triethylamine (287.2 mg, 2.84 mmol). Methanesulfonyl chloride (195 mg, 1.70 mmol) was then added via a syringe. The solution was stirred at room temperature for 4 h. Next, 50 mL of water was added and extracted with $CHCl_3$ (3 × 50 mL). The organic layer was dried over $MgSO_4$. After the solvent was removed, the residue was purified by silica gel chromatography to afford **90** (214 mg, 64%). ^{1}H NMR (400 MHz, $CDCL_3$): δ 7.70 (d, J = 15.8 Hz, 1H), 7.69 (d, J = 16.0 Hz, 1H), 7.58 (d, J = 3.1 Hz, 2H), 7.56 (d, J = 3.3 Hz, 2H), 7.31 (d, J = 8.5 Hz, 2H), 7.03 (d, J = 15.9 Hz, 1H), 6.97 (d, J = 15.8 Hz, 1H), 6.94 (d, J = 8.5 Hz, 2H), 4.44–4.29 (m, 2H), 4.23–4.02 (m, 2H), 3.91–3.79 (m, 2H), 3.79–3.75 (m, 2H), 3.74–3.64 (m, 4H), 3.29 (s, 3H), 3.05 (s, 3H), 1.48 (s, 9H). MS (ESI): m/z calcd for $C_{30}H_{39}NO_9S$, 589.23; found, 590.25 ($M + H^+$).

Radiolabeling. *Procedure for Labeling of [^{125}I]**6**, [^{125}I]**70**, and [^{125}I]**71**.* The radioiodinated ligands [^{125}I]**6**, [^{125}I]**70**, and [^{125}I]**71** were prepared from the corresponding tributyltin precursors through an iododestannylation reaction using hydrogen peroxide as an oxidant with radiochemical yields of 27.6, 15.3, and 24.1%, respectively. After purification by HPLC, the radiochemical purity of these ligands was greater than 98% [HPLC conditions: Waters 5C18-AR-II column (Analytical 4.6 mm × 150 mm) CH_3CN/H_2O = 6/4, 1 mL/min for **70**, CH_3CN/H_2O = 7/3, 1 mL/min for **71**, and CH_3CN/H_2O = 8/2, 1 mL/min for **6**]. The specific activity of the no carrier-added preparation was comparable to that of Na^{125}I, 2200 Ci/mmol. Finally, the radiochemical identity of the radioiodinated ligands was verified by coinjection with nonradioactive compounds using HPLC profiles. The final product was stored at −20 °C for autoradiography and biodistribution experiments.

*Procedure for Labeling of [^{18}F]**83** and [^{18}F]**85**.* [^{18}F]Fluoride was produced by the JSW typeBC3015 cyclotron via an $^{18}O(p,n)^{18}F$ reaction and passed through a Sep-Pak Light QMA cartridge (Waters) as an aqueous solution in ^{18}O-enriched water. The cartridge was dried by airflow, and the $^{18}F^-$ activity was eluted with a K_2CO_3 solution (33 mM). Kryptofix$_{222}$ (6–8 mg) was dissolved in the solution of [^{18}F]fluoride in water. The solvent was removed at 120 °C under a stream of nitrogen gas. The residue was azeotropically dried with 0.3 mL of anhydrous acetonitrile twice at 120 °C under a stream of nitrogen gas. For [^{18}F]**83**, a solution of the tosylate precursor **80** (1.0 mg) in DMSO (0.2 mL) was added to the reaction vessel containing the $^{18}F^-$ activity. The mixture was heated at 120 °C for 5 min. Water (3 mL) was added, and the mixture was passed through a preconditioned Sep-Pak Plus-C18 cartridge (Waters). The cartridge was washed with 10 mL of water, and the labeled compound was eluted with 2 mL of acetonitrile. The eluted compound was purified by semipreparative HPLC (Waters, 5C18-AR-II, 10 mm × 150 mm). The retention time of [^{18}F]**83** was 13.1 min in this HPLC system (CH_3CN/water = 7/3; flow rate = 4 mL/min). The preparation took 40 min, and the radiochemical yield was 49% (decay corrected). For [^{18}F]**85**, a solution of the mesylate precursor **90** (1.0 mg) in DMSO (0.2 mL) was added to the reaction vessel containing the $^{18}F^-$ activity. The mixture was heated at 120 °C for 5 min. Water (2 mL) was added, and the solution was cooled down for 1 min. HCl (1 M aqueous solution, 2 mL) was then added, and the mixture was heated at 120 °C again for 5 min. An aqueous solution of K_2CO_3 was added to adjust the pH to basic (pH 8–9). The mixture was extracted with ethyl acetate (1 mL × 2), the combined organic layer was dried (Na_2SO_4), and the solvent was removed. The residue was dissolved in CH_3CN and subjected to HPLC for purification (Waters, 5C18-AR-II, 10 mm × 150 mm, CH_3CN/water = 1/1; flow rate = 4 mL/min). The retention time of [^{18}F]**85** was 6.6 min in this HPLC system. The preparation took 80 min, and the radiochemical yield was 13% (decay corrected). The radiochemical purity of both tracers was greater than 98% with an estimated specific activity of 900–1500 Ci/mmol.

Binding Assay in Vitro Using Aβ Aggregates. Inhibition experiments were carried out in 12 mm × 75 mm borosilicate glass tubes according to procedures described previously with some modifications.[22] Briefly, 100 μL of aggregated Aβ fibrils (60 nM in the final assay mixture) was added to a mixture containing 100 μL of radioligands ([^{125}I]IMPY) at an appropriate concentration, 10 μL of inhibitors (10^{-5}–10^{-10} M in ethanol), and 790 μL of PBS (0.2 M, pH = 7.4) in a final volume of 1 mL. Nonspecific binding was defined in the presence of 1 μM IMPY. The mixture was incubated for 2 h at 37 °C with constant shaking, and then, the bound and free radioactive fractions were separated by vacuum filtration through borosilicate glass fiber filters (Whatman GF/B) using a M-24 cell harvester (Brandel, Gaithersburg, MD). The radioactivity from filters containing the bound ^{125}I ligand was measured in a γ-counter (WALLAC/Wizard 1470, United States) with 70% efficiency. Under the assay conditions, the specifically bound fraction accounted for about 10% of total radioactivity. The half maximal inhibitory concentration (IC_{50}) was determined using GraphPad Prism 4.0, and the inhibition constant (K_i) was calculated using the Cheng–Prusoff equation: $K_i = IC_{50}/(1 + [L]/K_d)$.[40]

Autoradiography in Vitro Using Tg Mouse Brains. Paraffin-embedded mouse brain sections (C57BL6-APP/PS1, 12 months old, male) and wild-type control mouse brain sections (C57BL6, 12 months old, male) were deparaffinized with 2 × 20 min washes in xylene, 2 × 5 min washes in 100% ethanol, a 5 min wash in 90% ethanol/H_2O, a 5 min wash in 80% ethanol/H_2O, a 5 min wash in 60% ethanol/H_2O, and a 10 min wash in running tap water, and then incubated in PBS (0.2 M, pH = 7.4) for 30 min. The sections were incubated with radiolabeled tracers (5 μCi/100 μL) for 1 h at room temperature, then washed with 40% ethanol for 3 min, and rinsed with water for 30 s. After they were dried, the labeled sections were exposed to a Fuji Film imaging plate overnight. The in vitro autoradiographic images were obtained using a BAS5000 scanner system (Fuji Film). The presence and location of plaques in the sections were confirmed with fluorescent staining using thioflavin S.

Autoradiography in Vitro Using Human AD Brains. Paraffin-embedded postmortem brain sections (Temporal lobe) of an AD patient (75 year old male) and normal control brain sections (20 year old male) were obtained from BioChain. The same protocol was employed as for the Tg mouse brains. Finally, the presence and location of plaques in the sections were confirmed with immunohistochemical staining using a monoclonal $A\beta_{1-42}$ antibody, BC05 (Wako).

Biodistribution Experiments in Vivo Using Normal ddY Mice. The biodistribution experiments were performed in normal female ddY mice (5 weeks, average weight, about 20 g) and approved by the animal care committee of Kyoto University. A saline solution containing the radiolabeled tracers (1 μCi/100 μL for radioiodinated tracers, 10 μCi/100 μL for radiofluorinated tracers) was injected directly into the tail. The mice were sacrificed at various time points

postinjection. The organs of interest were removed and weighed, and the radioactivity was measured with an automatic γ-counter (WALLAC/Wizard 1470). The percent dose per gram of wet tissue was calculated by a comparison of the tissue counts to suitably diluted aliquots of the injected material.

Determination of the Partition Coefficient. The partition coefficients for these radiolabeled compounds were determined as described previously but with some modifications.[41] The radiolabeled compound (10 μCi) was added to a premixed suspensions containing 3 g of *n*-octanol and 3 g of PBS (0.05 M, pH = 7.4) in a test tube. The test tube was vortexed for 3 min at room temperature and centrifuged for 5 min at 3000 rpm. Two weighted samples from the *n*-octanol (100 μL) and buffer (500 μL) layers were measured. The partition coefficient was expressed as the logarithm of the ratio of the count per gram from *n*-octanol versus PBS. Samples from the *n*-octanol layer were repartitioned until consistent partition coefficient values were obtained. The measurement was done in triplicate and repeated three times.

■ ASSOCIATED CONTENT

Supporting Information. Purity of key target compounds together with HPLC chromatograms, ^{1}H NMR spectra of compounds, and HRMS data of key target compounds. This material is available free of charge via the Internet at http://pubs.acs.org.

■ AUTHOR INFORMATION

Corresponding Author

*Tel: +81-75-753-4608. Fax: +81-75-753-4568. E-mail: ono@pharm.kyoto-u.ac.jp (M.O.). Tel: +81-75-753-4556. Fax: +81-75-753-4568. E-mail: hsaji@pharm.kyoto-u.ac.jp (H.S.).

■ ACKNOWLEDGMENT

This study was supported by a Grant-in-aid for Young Scientists (A) and Exploratory Research from the Ministry of Education, Culture, Sports, Science and Technology, Japan. This study was also supported by the China Scholarship Council (CSC).

■ ABBREVIATIONS USED

AD, Alzheimer's disease; Aβ, β-amyloid; NFTs, neurofibrillary tangles; PET, positron emission tomography; SPECT, single photon emission computed tomography; ThT, thioflavin T; CR, Congo Red; BBB, blood–brain barrier; SAR, structure–activity relationship; TBDMSCl, *tert*-butyldimethylsilyl chloride; BOC, butyloxycarbonyl; DMSO, dimethyl sulfoxide; HPLC, high-performance liquid chromatography; THF, tetrahydrofuran; TBAF, tetra-*n*-butylammonium fluoride; FPEG, fluoro-pegylated; Tg, transgenic; IMSB, 1-iodo-2,5-bis(3-hydroxycarbonyl-4-methoxy) styrylbenzene

■ REFERENCES

(1) Selkoe, D. J. The origins of Alzheimer disease: A is for amyloid. *J. Am. Med. Assoc.* **2000**, *283*, 1615–1617.

(2) Selkoe, D. J. Alzheimer's disease: Genes, proteins, and therapy. *Physiol. Rev.* **2001**, *81*, 741–766.

(3) Hardy, J. A.; Higgins, G. A. Alzheimer's disease: The amyloid cascade hypothesis. *Science* **1992**, *256*, 184–185.

(4) Hardy, J. A.; Selkoe, D. J. The amyloid hypothesis of Alzheimer's disease: Progress and problems on the road to therapeutics. *Science* **2002**, *297*, 353–356.

(5) Klein, W. L.; Krafft, G. A.; Finch, C. E. Targeting small Aβ oligomers: The solution to an Alzheimer's disease conundrum? *Trends Neurosci.* **2001**, *24*, 219–224.

(6) McLean, C. A.; Cherny, R. A.; Fraser, F. W.; Fuller, S. J.; Smith, M. J.; Beyreuther, K.; Bush, A. I.; Masters, C. L. Soluble pool of Aβ amyloid as a determinant of severity of neurodegeneration in Alzheimer's disease. *Ann. Neurol.* **1999**, *46*, 860–866.

(7) Nelson, P. T.; Braak, H.; Markesbery, W. R. Neuropathology and cognitive impairment in Alzheimer disease: A complex but coherent relationship. *J. Neuropathol. Exp. Neurol.* **2009**, *68*, 1–14.

(8) Näslund, J.; Haroutunian, V.; Mohs, R.; Davis, K. L.; Davies, P.; Greengard, P.; Buxbaum, J. D. Correlation between elevated levels of amyloid β-peptide in the brain and cognitive decline. *J. Am. Med. Assoc.* **2000**, *283*, 1571–1577.

(9) Sorrentino, G.; Bonavita, V. Neurodegeneration and Alzheimer's disease: The lesson from tauopathies. *J. Neurol. Sci.* **2007**, *28*, 63–71.

(10) Skovronsky, D. M.; Lee, V. M.; Trojanowski, J. Q. Neurodegenerative Diseases: New concepts of pathogenesis and their therapeutic implications. *Annu. Rev. Pathol.: Mech. Dis.* **2006**, *1*, 151–170.

(11) Mathis, C. A.; Wang, Y.; Klunk, W. E. Imaging β-amyloid plaques and neurofibrillary tangles in the aging human brain. *Curr. Pharm. Des.* **2004**, *10*, 1469–1492.

(12) Cai, L. S.; Innis, R. B.; Pike, V. W. Radioligand development for PET imaging of β-amyloid (Aβ)-current status. *Curr. Med. Chem.* **2007**, *14*, 19–52.

(13) Mathis, C. A.; Wang, Y.; Holt, D. P.; Huang, G. F.; Debnath, M. L.; Klunk, W. E. Synthesis and evaluation of ^{11}C-labeled 6-substituted 2-arylbenzothiazoles as amyloid imaging agents. *J. Med. Chem.* **2003**, *46*, 2740–2754.

(14) Klunk, W. E.; Engler, H.; Nordberg, A.; Wang, Y.; Blomqvist, G.; Holt, D. P.; Bergstrom, M.; Savitcheva, I.; Huang, G. F.; Estrada, S.; Ausen, B.; Debnath, M. L.; Barletta, J.; Price, J. C.; Sandell, J.; Lopresti, B. J.; Wall, A.; Koivisto, P.; Antoni, G.; Mathis, C. A.; Langstrom, B. Imaging brain amyloid in Alzheimer's disease with Pittsburgh Compound-B. *Ann. Neurol.* **2004**, *55*, 306–319.

(15) Koole, M.; Lewis, D.; Buckley, C.; Nelissen, N.; Vandenbulcke, M.; Brooks, D. J.; Vandenberghe, R.; Laere, K. V. Whole-body biodistribution and radiation dosimetry of ^{18}F-GE067: A radioligand for in vivo brain amyloid imaging. *J. Nucl. Med.* **2009**, *50*, 818–822.

(16) Rowe, C. C.; Ackerman, U.; Browne, W.; Mulligan, R.; Pike, K. L.; O'Keefe, G.; Tochon-Danguy, H.; Chan, G.; Berlangieri, S. U.; Jones, G.; Dickinson-Rowe, K. L.; Kung, H. F.; Zhang, W.; Kung, M. P.; Skovronsky, D.; Dyrks, T.; Holl, G.; Krause, S.; Friebe, M.; Lehman, L.; Lindemann, S.; Dinkelborg, L. M.; Masters, C. L.; Villemagne, V. L. Imaging of amyloid β in Alzheimer's disease with ^{18}F-BAY94-9172, a novel PET tracer: proof of mechanism. *Lancet Neurol.* **2008**, *7*, 129–135.

(17) Choi, S. R.; Golding, G.; Zhuang, Z. P.; Zhang, W.; Lim, N.; Hefti, F.; Benedum, T. E.; Kilbourn, M. R.; Skovronsky, D.; Kung, H. F. Preclinical properties of ^{18}F-AV-45: A PET agent for Aβ plaques in the brain. *J. Nucl. Med.* **2009**, *50*, 1887–1894.

(18) Kung, H. F.; Choi, S. R.; Qu, W. C.; Zhang, W.; Skovronsky, D. ^{18}F stilbenes and styrylpyridines for PET imaging of Aβ plaques in Alzheimer's disease: A miniperspective. *J. Med. Chem.* **2010**, *53*, 933–941.

(19) Kung, M. P.; Hou, C.; Zhuang, Z. P.; Zhang, B.; Skovronsky, D.; Trojanowski, J. Q.; Lee, V. M.; Kung, H. F. IMPY: An improved thioflavin-T derivative for in vivo labeling of β-amyloid plaques. *Brain Res.* **2002**, *956*, 202–210.

(20) Zhuang, Z. P.; Kung, M. P.; Wilson, A.; Lee, C. W.; Plossl, K.; Hou, C.; Holtzman, D. M.; Kung, H. F. Structure-activity relationship of imidazo[1,2-a]pyridines as ligands for detecting β-amyloid plaques in the brain. *J. Med. Chem.* **2003**, *46*, 237–243.

(21) Newberg, A. B.; Wintering, N. A.; Plossl, K.; Hochold, J.; Stabin, M. G.; Watson, M.; Skovronsky, D.; Clark, C. M.; Kung, M. P.; Kung, H. F. Safety, biodistribution, and dosimetry of ^{123}I-IMPY: A novel amyloid plaque-imaging agent for the diagnosis of Alzheimer's disease. *J. Nucl. Med.* **2006**, *47*, 748–754.

(22) Qu, W. C.; Kung, M. P.; Hou, C.; Benedum, T. E.; Kung, H. F. Novel styrylpyridines as probes for SPECT imaging of amyloid plaques. *J. Med. Chem.* **2007**, *50*, 2157–2165.

(23) Watanabe, H.; Ono, M.; Haratake, M.; Kobashi, M.; Saji, H.; Nakayama, M. Synthesis and characterization of novel phenylindoles as potential probes for imaging of β-amyloid plaques in the brain. *Bioorg. Med. Chem.* **2010**, *18*, 4740–4746.

(24) Cui, M. C.; Ono, M.; Kimura, H.; Kawashima, H.; Liu, B. L.; Saji, H. Radioiodinated benzimidazole derivatives as single photon emission computed tomography probes for imaging of β-amyloid plaques in Alzheimer's disease. *Nucl. Med. Biol.* DOI: 10.1016/j.nucmedbio.2010.09.012.

(25) Lockhart, A.; Ye, L.; Judd, D. B.; Merritt, A. T.; Lowe, P. N.; Morgenstern, J. L.; Hong, G.; Gee, A. D.; Brown, J. Evidence for the presence of three distinct binding sites for the thioflavin T class of Alzheimer's disease PET imaging agents on beta-amyloid peptide fibrils. *J. Biol. Chem.* **2005**, *280*, 7677–7684.

(26) Ono, M.; Yoshida, N.; Ishibashi, K.; Haratake, M.; Arano, Y.; Mori, H.; Nakayama, M. Radioiodinated flavones for in vivo imaging of β-amyloid plaques in the brain. *J. Med. Chem.* **2005**, *48*, 7253–7260.

(27) Ono, M.; Watanabe, R.; Kawashima, H.; Kawai, T.; Watanabe, H.; Haratake, M.; Saji, H.; Nakayama, M. ^{18}F-Labeled flavones for in vivo imaging of β-amyloid plaques in Alzheimer's brains. *Bioorg. Med. Chem.* **2009**, *17*, 2069–2076.

(28) Ono, M.; Haratake, M.; Mori, H.; Nakayama, M. Novel chalcones as probes for in vivo imaging of β-amyloid plaques in Alzheimer's brains. *Bioorg. Med. Chem.* **2007**, *15*, 6802–6809.

(29) Ono, M.; Watanabe, R.; Kawashima, H.; Cheng, Y.; Kimura, H.; Watanabe, H.; Haratake, M.; Saji, H.; Nakayama, M. Fluoro-pegylated chalcones as positron emission tomography probes for in vivo imaging of β-amyloid plaques in Alzheimer's disease. *J. Med. Chem.* **2009**, *52*, 6394–6401.

(30) Ono, M.; Maya, Y.; Haratake, M.; Ito, K.; Mori, H.; Nakayama, M. Aurones serve as probes of β-amyloid plaques in Alzheimer's disease. *Biochem. Biophys. Res. Commun.* **2007**, *361*, 116–121.

(31) Maya, Y.; Ono, M.; Watanabe, H.; Haratake, M.; Saji, H.; Nakayama, M. Novel radioiodinated aurones as probes for SPECT imaging of β-amyloid plaques in the brain. *Bioconjugate Chem.* **2009**, *20*, 95–101.

(32) Ryu, E. K.; Choe, Y. S.; Lee, K. H.; Choi, Y.; Kim, B. T. Curcumin and dehydrozingerone derivatives: Synthesis, radiolabeling, and evaluation for β-amyloid plaque imaging. *J. Med. Chem.* **2006**, *49*, 6111–6119.

(33) Price, L. C.; Buescher, R. W. Kinetics of alkaline degradation of the food pigments curcumin and curcuminoids. *J. Food Sci.* **2006**, *62*, 267–269.

(34) Tonnesen, H. H.; Karlsen, J. Studies on curcumin and curcuminoid. VI. Kinetics of curcumin degradation in aqueous solution. *Z. Lebensm.-Unters. Forsch. A* **1985**, *180*, 402–404.

(35) Van Der Goot, H. The chemistry and qualitative structure-activity relationship of curcumin. In Recent development in Curcumin Pharmacochemistry. *Proc. Int. Symp. Curcumin Pharmacochemistry (ISCP)* **1995**, 23–33.

(36) Zhang, W.; Kung, M. P.; Oya, S.; Hou, C.; Kung, H. F. 18F-labeled styrylpyridines as PET agents for amyloid plaque imaging. *Nucl. Med. Biol.* **2007**, *34*, 89–97.

(37) Zhang, W.; Oya, S.; Kung, M. P.; Hou, C.; Maier, D. L.; Kung, H. F. F-18 polyethyleneglycol stilbenes as PET imaging agents targeting Aβ aggregates in the brain. *Nucl. Med. Biol.* **2005**, *32*, 799–809.

(38) Stephenson, K. A.; Chandra, R.; Zhuang, Z. P.; Hou, C.; Oya, S.; Kung, M. P.; Kung, H. F. Fluoro-pegylated (FPEG) imaging agents targeting Aβ aggregates. *Bioconjugate Chem.* **2007**, *18*, 238–246.

(39) Zhuang, Z. P.; Kung, M. P.; Hou, C.; Skovronsky, D. M.; Gur, T. L.; Plossl, K.; Trojanowski, J. Q.; Lee, V. M. Y.; Kung, H. F. Radioiodinated styrylbenzenes and thioflavins as probes for amyloid aggregates. *J. Med. Chem.* **2001**, *44*, 1905–1914.

(40) Cheng, Y.; Prusoff, W. Relationship between the inhibition constant (Ki) and the concentration of inhibitor which causes 50% inhibition (I50) of an enzymatic reaction. *Biochem. Pharmacol.* **1973**, *22*, 3099–3108.

(41) Wu, C. Y.; Wei, J. J.; Gao, K. Q.; Wang, Y. M. Dibenzothiazoles as novel amyloid-imaging agents. *Bioorg. Med. Chem.* **2007**, *15*, 2789–2796.

POTENTIAL CLINICAL RELEVANCE

Nanomedicine: Nanotechnology, Biology, and Medicine
7 (2011) 638–646

Research Article

nanomedjournal.com

Effective encapsulation of a new cationic gadolinium chelate into apoferritin and its evaluation as an MRI contrast agent

Akira Makino, PhD[a], Hiroshi Harada, PhD[b], Tomohisa Okada, MD, PhD[c], Hiroyuki Kimura, PhD[d], Hiroo Amano, PhD[d], Hideo Saji, PhD[d], Masahiro Hiraoka, MD, PhD[e], Shunsaku Kimura, PhD[a,*]

[a]*Department of Material Chemistry, Graduate School of Engineering, Kyoto University, Kyoto-Daigaku-Katsura, Nishikyo-ku, Kyoto, Japan*
[b]*Group of Radiation and Tumor Biology, Career-Path Promotion Unit for Young Life Scientists, Kyoto University, Kyoto, Japan*
[c]*Department of Diagnostic Imaging and Nuclear Medicine, Graduate School of Medicine, Kyoto University, Kyoto, Japan*
[d]*Department of Patho-Functional Bioanalysis, Graduate School of Pharmaceutical Sciences, Kyoto University, Kyoto, Japan*
[e]*Department of Radiation Oncology and Image-applied Therapy, Graduate School of Medicine, Kyoto University, Kyoto, Japan*

Received 7 December 2010; accepted 24 January 2011

Abstract

Gd-Me_2DO2A with a T_1 proton relaxivity twice as high as that of commercial Gd-DOTA was newly designed and synthesized. Me_2DO2A kept its high association property with gadolinium ions (Gd^{3+}), and the Gd-Me_2DO2A was efficiently encapsulated into the apoferritin cavity to further enhance the T_1 relaxivity as much as 10-fold higher than Gd-DOTA on a Gd basis. The high T_1 relaxivity was attained by (i) increased accessibility of water molecules to Gd^{3+} ions in the chelate and (ii) macromolecular effect of the encapsulation. By the surface modification of apoferritin with dextran, in vivo blood clearance time of apoferritin could be prolonged. Magnetic resonance imaging of tumor-bearing mice showed that the apoferritin contrast agent accomplished tumor detection effectively as a bright signal as a result of the enhanced permeation and retention effect. Single-dose toxicity test showed no serious side effects. The apoferritin-encapsulated Gd is therefore a possible candidate for a new magnetic resonance imaging contrast agent.

From the Clinical Editor: In this study by Makino et al, a novel encapsulation method of a cationic Gd chelate with apoferritin led to a proton relaxivity 10 times higher than that of standard clinically used Gd contrast dyes. If this complex passed toxicity studies, it would have an enormous clinical significance in providing a much more sensitive method to visualize BBB breakdown.

Key words: Magnetic resonance imaging; Molecular imaging; Apoferritin; Drug delivery; Gadolinium complex

High-contrast magnetic resonance (MR) images for precise diagnosis can be obtained in the presence of a MR imaging (MRI) contrast agent (CA), which accelerates relaxation of surrounding proton signals.[1,2] MRI CAs are normally divided into two types according to the mechanism of the contrast improvement; one is shortening of the longitudinal (T_1) relaxation time of water protons,[1] and the other is shortening of transverse (T_2) relaxation time.[2] Gadolinium (Gd) ion is a well-known T_1-shortening reagent, because Gd possesses seven unshared electrons. However, free Gd^{3+} is easily replaced with Ca^{2+} and Mg^{2+} in body, showing some toxicity.[3,4] Therefore, Gd chelates such as Gd-DOTA and Gd-DTPA are used for medical applications (Figure 1, *A* and *B*).[1] The intrinsic proton relaxivity of Gd ion is decreased by the chelate formation, resulting in the need to administer large amounts of the Gd chelate for each imaging, which increases the risk of side effects.[5]

We consider two strategies to increase proton relaxivity of Gd chelates, which leads to reduction in the dosage necessary to achieve MRI contrast: (i) increase of the water-accessible sites on Gd, and (ii) improve the macromolecular effect to increase the rotational correlation time. Further, we take care not to impair the high association constant of the chelate with Gd^{3+} for toxicity reduction and also not to shorten the T_2 value to avoid signal broadening.

The conventional chelator for Gd^{3+}, DOTA (1,4,7,10-tetra-azacyclododecane-1,4,7,10-tetraacetic acid), possesses eight coordination sites in the aza-crown structure of four carboxylates and four nitrogen atoms. We removed two carboxylates from

This study was conducted as a part of the project, "R&D of Molecular Imaging Equipment for Malignant Tumor Therapy Support," supported by NEDO (New Energy and Industrial Technology Development Organization).
*Corresponding author:
E-mail address: shun@scl.kyoto-u.ac.jp (S. Kimura).

1549-9634/$ – see front matter © 2011 Elsevier Inc. All rights reserved.
doi:10.1016/j.nano.2011.01.015

Please cite this article as: A. Makino, et al, Effective encapsulation of a new cationic gadolinium chelate into apoferritin and its evaluation as an MRI contrast agent. *Nanomedicine: NBM* 2011;7:638-9, doi:10.1016/j.nano.2011.01.015

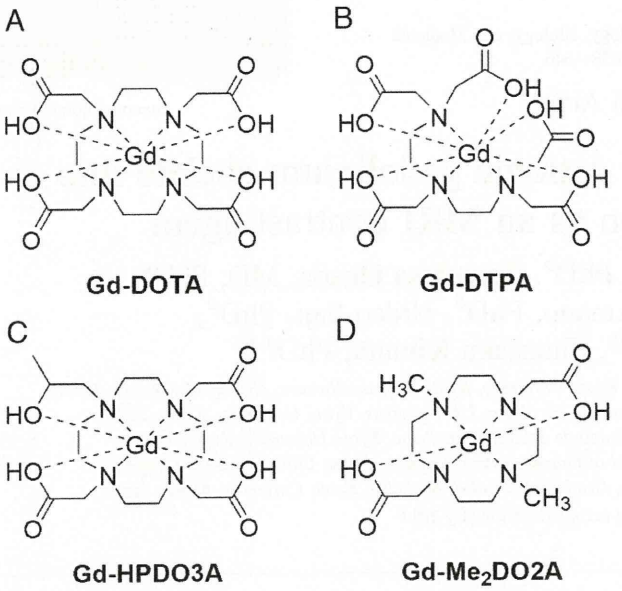

Figure 1. Chemical structures of Gd-based MRI CAs: **(A)** Gd-DOTA, **(B)** Gd-DTPA, **(C)** Gd-HPDO3A, and **(D)** Gd-Me_2DO2A.

DOTA for the increase in hydration sites, but put two methyl groups at the two nitrogen atoms for enhancement of Gd^{3+} coordination ability.

The rotational correlation time of chromophores can be increased by binding to macromolecules. Thus, we encapsulated Gd chelates in a protein capsule, apoferritin, which is known to condense some cations to the cavity. The newly designed Gd chelate was cationic so as to be encapsulated into apoferritin cavity by electrostatic interactions. Immobilization via the secondary interaction may allow moderate motions of the Gd chelate on the inner surface to prevent the excess shortening of the T_2 relaxation time.

At the tumor regions, submicron-size defects exist on blood vessel walls because of accelerated blood vessel formation, enabling macromolecules to leak out through the wall. Moreover, the lymphatic system around tumor tissues grows too slowly to exclude foreign compounds from tumor tissues. Molecular assemblies with diameters of several dozen nanometers accumulate at tumor regions and could be utilized as nanocarriers for tumor imaging.[6,7] This effect is called the enhanced permeability and retention (EPR) effect.[8-10]

In this study we examined strategies to improve the MRI CA sensitivity and EPR effect-based tumor imaging through utilizing apoferritin as a nano-ordered carrier.

Methods

All reagents and solvents were purchased commercially and used as received unless otherwise noted. Apoferritin was purchased from EMD Biosciences, Inc. (Gibbstown, New Jersey) and used without further purification (lot no. D00049186).

Preparation and evaluation of the apoferritin MRI CA are summarized in the Supplementary Materials, available online at http://www.nanomedjournal.com.

Measurements

Nuclear MR and ultraviolet spectra were recorded with a Bruker DPX400 (Billerica, Massachusetts) and Shimadzu UV-2450 spectrometer (Kyoto, Japan), respectively. Transmission electron microscopy (TEM) images were taken using a JEOL JEM-200 EXII transmission electron microscope (JEOL, Tokyo, Japan). For the observation, a drop of dispersion was mounted on a carbon-coated copper grid and stained negatively with 2 wt% uranyl acetate, followed by suction of the excess fluid with a filter paper. Apoferritin concentration was estimated using the Lowry method, and apoferritin standard solutions were used to prepare the calibration curve. Gd concentration was determined by inductively coupled plasma emission-atomic emission spectrophotometry (ICP-AES SPS4000; Seiko Instruments Inc., Chiba, Japan). The Gd emission intensity in ICP-AES was calibrated at 342.247 nm. A calibration curve was constructed using Gd $(NO_3)_3$ solutions with concentrations of 0.5−100 ppm, which were prepared by diluting standard $Gd(NO_3)_3$ nitrate solutions (Wako Pure Chemical Industries, Ltd., Osaka, Japan) with deionized water. MRI was carried out using a 1.5-T Toshiba MRI system (EXCELART Vantage Toshiba, Tochigi, Japan). Optical imaging experiments were carried out using an IVIS-200 in vivo imaging device (Xenogen, Alameda, California).

Ethics

All of our in vivo animal experiments were approved by the Animal Research Committee of Kyoto University. Animals were treated humanely.

Results

Design of a new MRI CA, Gd-Me_2DO2A

Apoferritin is an apoprotein that consists of 24 protein subunits of two types (heavy and light chains), and forms a hollow cagelike structure with a diameter of ~13 nm. It can encapsulate up to 4500 iron atoms in the form of ferric oxyhydroxide and works in our living system as an iron storage protein named ferritin.[11-15] We chose apoferritin as a nano-ordered carrier for Gd-based MRI CA delivery.

Apoferritin MRI CA, which contains Gd chelate in the cavity, was previously reported by Aime et al.[16] The group encapsulated the electrically neutral Gd chelate Gd-HPDO3A (Figure 1, *C*). However, an excess amount of Gd-HPDO3A, which is a 10,000-fold larger amount than apoferritin, was needed to encapsulate only 8–10 Gd chelates per apoferritin molecule, which means its encapsulation efficiency is low. To improve the encapsulation efficiency, we focused our attention on the intrinsic property of apoferritin to condense cations in the cavity.[14,15,17] A positively charged Gd chelate, Gd-Me_2DO2A, was therefore designed by reduction of the number of carboxylates in the chelator from the conventional chelators of Gd-DOTA, Gd-DTPA, and Gd-HPDO3A (Figure 1). The net charge of Gd-Me_2DO2A is +1, leaving three coordination sites for water molecules, which should also contribute to the improvement of proton relaxivity of the chelated Gd.

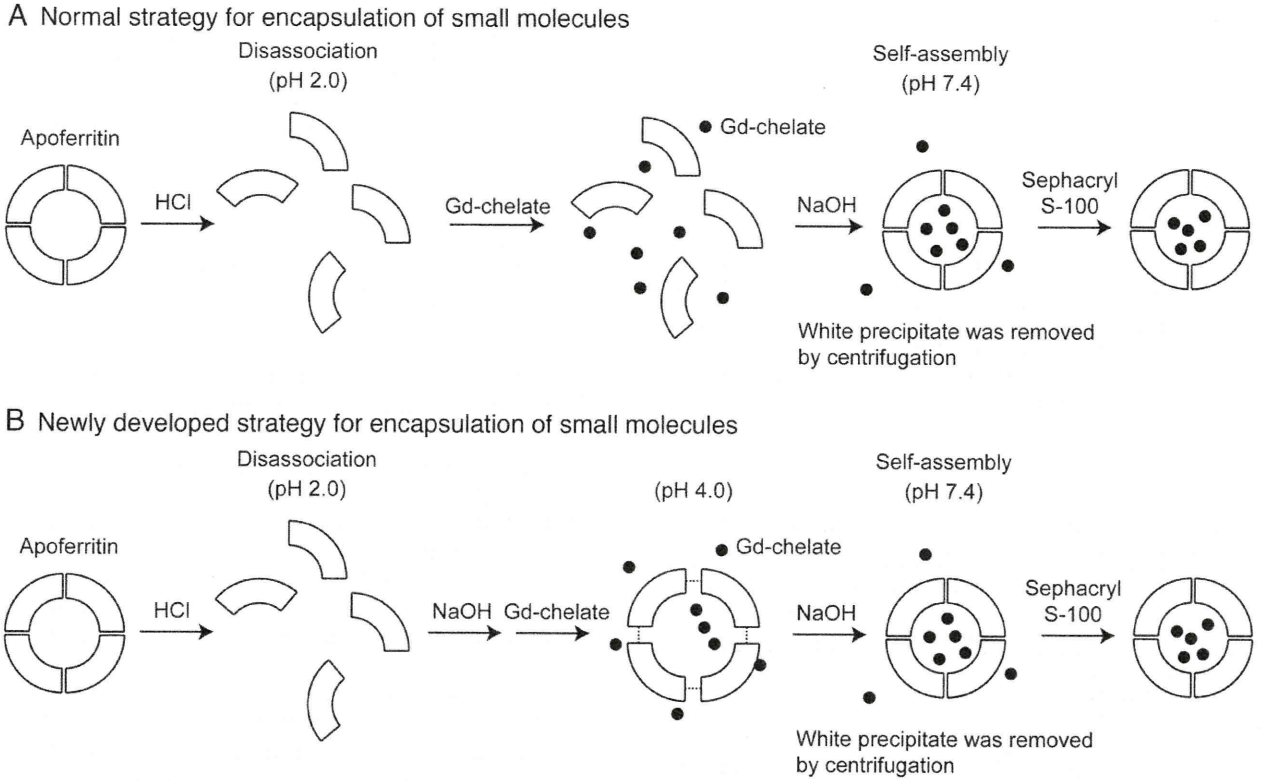

Figure 2. **(A)** Conventional strategy to encapsulate small molecules into apoferritin cavity. **(B)** Newly developed strategy.

Preparation of a new cationic Gd chelate, Gd-Me_2DO2A

Starting from 1,4,7,10-tetraazacyclododecane, Gd-Me_2DO2A was synthesized (Supplementary Figure S1, available online at http://www.nanomedjournal.com). The thermodynamic stability constant (log K_{ML}) of the new Gd chelate Gd-Me_2DO2A was 18.2, as determined by the conventional method using arsenazo III.[18,19] Thermodynamic Gd stability constants of Gd-DOTA,[19] Gd-DTPA[20], and Gd-DTPA-BMA,[20] which are commercially available with US Food and Drug Administration approval, are reported to be 24, 18, and 15, respectively. Gd-Me_2DO2A therefore maintains a thermodynamic stability as high as commercially available chelates, despite fewer carboxylates in the chelate. The reported thermodynamic Gd stability constant of DO2A, having no *N*-methyl group, is 13[21] (the other group reported to be 19,[22] but this value is uncertain, because the stability constant with Ca^{2+} from the same group was corrected). The Gd stability constant of Me_2DO2A is thus higher than that of DO2A as a result of the contribution of the two *N*-methyl groups, which may strengthen the coordination ability of the aza-crown nitrogen atoms.

Phantom MR images of Gd-Me_2DO2A with changing concentrations are shown together with those of Gd-DOTA in Supplementary Figure S2. Images of Gd-Me_2DO2A are brighter than those of Gd-DOTA at lower concentrations. Proton relaxivities of Gd-DOTA and Gd-Me_2DO2A in water are 3.9 and 7.2, respectively, which are obtained as the solvent longitudinal relaxation time (T_1) by the inversion recovery method. This enhanced relaxivity of Gd-Me_2DO2A is due to the increased water coordination number from Gd-DOTA of 1 to Gd-Me_2DO2A of 3 per Gd ion.

Encapsulation of Gd chelate into apoferritin

Apoferritin has 14 ion channels of 3–4 Å in diameter, through which ferric ions and water molecules can move in and out in vivo. However, the diameter of Gd-Me_2DO2A is larger than that of the apoferritin ion channel, thus blocking the Gd chelate from passing through the channel.[23,24] Previously, Gd-HPDO3A was encapsulated in apoferritin, utilizing its pH-responsive behaviors of dissociating at pH 2.0 and reassembling at pH 7.4 (Figure 2, *A*).[25,26] Adopting the same method, Gd^{3+}, Gd-DOTA, and Gd-Me_2DO2A were encapsulated in apoferritin (Table 1). Concentrations of apoferritin and Gd after the encapsulation process were determined by the Lowry method[27] and by ICP measurements, respectively. When Gd^{3+} was added at pH 2.0 (entry 2, Table 1), apoferritin was precipitated. It is probable that some specific residues that are essential for apoferritin reassembling via hydrogen bond formation and electrostatic interaction were blocked by Gd^{3+}. Gd-DOTA and cationic Gd-Me_2DO2A did not yield as much precipitate as Gd^{3+}, but anionic Gd-DOTA was scarcely encapsulated in apoferritin (entry 3, Table 1). On the other hand, the concentration of the encapsulated Gd-Me_2DO2A in apoferritin became 1.5-fold higher than that of the feed solution (entry 4, Table 1), implying active condensation. The electrostatic interaction between the

Table 1
Encapsulation results of Gd chelate utilizing conventional strategy as illustrated in Figure 2, *A*

Entry	Gd chelate	Molar feed ratio of Gd chelate to apoferritin	Protein recovery rate (%)	Gd atoms per apoferritin molecule*
1	Gd-HPDO3A	10,000	-†	~10 (7.0)[19]
2	Gd^{3+}	10,000	6	8.2 (7.0)
3	Gd-DOTA	10,000	23	0.5 (7.0)
4	Gd-Me_2DO2A	10,000	25	10.8 (7.0)
5	Gd-Me_2DO2A	120	51	-‡ (0.2)

* Theoretical amount without condensation is shown in parentheses.
† Protein (apoferritin) recovery rate was not reported.
‡ Gd signal measured by ICP-AES was too weak, and Gd concentration in the solution could not be determined.

Table 2
Results of encapsulation of Gd chelate into apoferritin utilizing newly developed strategy as illustrated in Figure 2, *B*

Entry	Gd chelate	Molar feed ratio of Gd chelate to apoferritin	Protein recovery rate (%)	Gd atoms per apoferritin molecule*
6	Gd-Me_2DO2A	12	99	12.4 (0.02)
7	Gd-Me_2DO2A	48	97	21.1 (0.08)
8	Gd-Me_2DO2A	72	98	25.6 (0.12)
9	Gd-Me_2DO2A	120	98	36.2 (0.2)
10	Gd-Me_2DO2A	240	84	11.1 (0.4)
11	Gd-DOTA	120	100	0.3 (0.2)
12	Gd-DOTA	240	98	0.4 (0.4)
13	Gd-HPDO3A	120	97	0.2 (0.2)
14	Gd-HPDO3A	240	99	0.2 (0.4)

* Theoretical amount without condensation is shown in parentheses.

cationic Gd-Me_2DO2A and the anionic inner surface of apoferritin should work partially. However, the protein (apoferritin) recovery rate and the amounts of the encapsulated Gd chelates were relatively low.

We speculate that the main reason for the low protein recovery rate is production of irregular assembly during the reassembling process. In fact, there is a report that doxorubicin molecules bound to apoferritin subunits in the pH region of 3–4 lost an average of 48% apoferritin.[25] It was shown that the subunits start to reassemble at pH 3.0 to yield dimers predominantly at pH 3.5,[28] and apoferritin subunits form incomplete globular assembly via weak intersubunit interactions at pH 4.0. On the basis of these reports, we modified the reassembling process, wherein the apoferritin solution at pH 2.0 was titrated slowly by sodium hydroxide to reach 4.0, and then Gd chelate was added, followed by adjustment of the pH at 7.4 (Figure 2, *B*).

As summarized in Table 2, the protein recovery rates were drastically improved over 90%, and Gd-Me_2DO2A was highly condensed in the apoferritin cavity. The concentrations of Gd-Me_2DO2A in the cavity were evaluated to be 28- to 620-fold higher than those in the feed solutions (Table 2, entries 6–10). When encapsulation of Gd-Me_2DO2A was performed by the conventional method under the same condition as entry 9, a white precipitate was produced and the amount of Gd-Me_2DO2A encapsulated in apoferritin was extremely low (Table 1, entry 5).

Table 3
Evaluation of adsorbed Gd chelate on outer surface of apoferritin

Entry	Gd chelate	Molar feed ratio of Gd chelate to apoferritin	White precipitate (%)	Gd atoms per apoferritin molecule
15	Gd-DOTA	120	0	0.1
16	Gd-DOTA	10,000	0	0.2
17	Gd-HPDO3A	120	0	0.1
18	Gd-HPDO3A	10,000	0	0.1
19	Gd-Me_2DO2A	120	0	2.6
20	Gd-Me_2DO2A	10,000	91	8.8

This result is good evidence for the superiority of the present reconstruction and encapsulation process. Furthermore, integrity and capsule structure of the reconstructed apoferritin with Gd-Me_2DO2A in the cavity was confirmed by TEM observation (Supplementary Figure S3). When the Gd-Me_2DO2A feed ratio against apoferritin exceeded 240, a white precipitate was formed to decrease the protein recovery rate. At the same time, the amount of Gd-Me_2DO2A encapsulated in each apoferritin cavity became low (Table 2, entry 10). With increasing Gd chelates in the feed, the reassembling process may be disturbed by adsorption of Gd chelates onto some residues important for apoferritin reassembling.

Gd chelates were mixed with an intact apoferritin solution at pH 7.4, and apoferritin was separated by ultrafiltration. The concentrations of Gd and protein in the purified fraction were evaluated using ICP and the Lowry method, respectively (Table 3). When Gd-DOTA and Gd-HPDO3A were mixed with apoferritin, the amounts of Gd in the apoferritin fractions were low independent of the Gd chelate feed ratio (Table 3, entries 15–18). On the other hand, when Gd-Me_2DO2A of 120 eq against an apoferritin molecule was mixed with apoferritin, 2.6 Gd atoms per apoferritin was detected (Table 3, entry 19). As described above, the diameter of the apoferritin ion channel is not large enough to allow passage of Gd chelates, and Gd-Me_2DO2A cannot enter the apoferritin cavity without apoferritin disassociation. The zeta potential of apoferritin was found to be −18.9 mV. Therefore, Gd-Me_2DO2A is considered to be adsorbed onto the apoferritin outer surface by electrostatic interaction. However, the amount of Gd-Me_2DO2A adsorbed on the outer surface was as low as ~7% compared with that in the apoferritin cavity of 46.2 Gd atoms (Table 2, entry 9). Repeated washing of the apoferritin solution by ultrafiltration could not remove the Gd-Me_2DO2A, suggesting that Gd-Me_2DO2A was stably adsorbed on the surface.

Surface modification of apoferritin with dextran

Apoferritin on its own has a strong tendency to accumulate in liver, which is not suited for selective delivery of the encapsulated Gd chelate in apoferritin to tumor tissues. Therefore, after Gd chelates were encapsulated into the apoferritin cavity, the apoferritin outer surface was modified by partially oxidized dextran to prolong in vivo blood clearance time (Figure 3).[29,30] The diameter of the resulting apoferritin could be easily controlled from 30 to 100 nm with changing the activation degree of dextran by cyanogen bromide, and set here to be 30 nm.

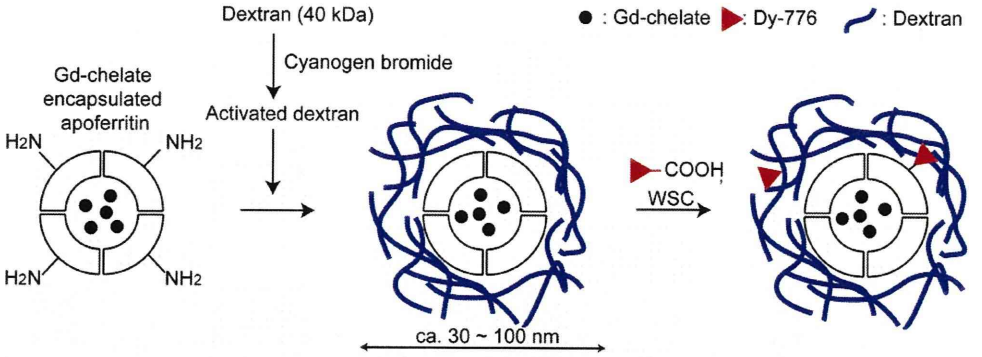

Figure 3. Surface modification of apoferritin. WSC, water-soluble carbodiimide.

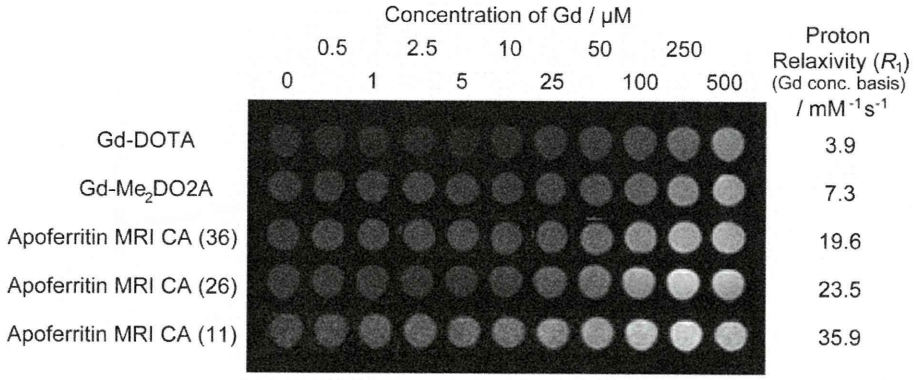

Figure 4. MR images of Gd-DOTA, Gd-Me_2DO2A, and apoferritin CA encapsulating Gd-Me_2DO2A under various concentrations, and their proton relaxivities. Horizontal axis represents Gd molar concentration; numbers of encapsulated Gd-Me_2DO2A molecules in each apoferritin cavity are shown in parentheses. Proton relaxivity of each CA on a Gd molar concentration basis, as determined by the inversion recovery method, is shown in the right column. Phantom image was taken by 1.5-T MRI equipment with T_R = 500 msec and T_E = 15 msec.

To the dextran-coated apoferritin molecule was attached the near-infrared fluorescence (NIRF) compound Dyomics Dy-776 (Dyomics GmbH, Jena, Germany) so as to trace directly the in vivo distribution of apoferritin. Suppression of apoferritin entrapment at liver was proven by the NIRF imaging technique as shown in Supplementary Figure S4. The suppressed accumulation in liver is due to the dextran coating, which blinds the nature of apoferritin and also endows the surface with a hydration layer similarly to PEGylated nano-carriers.[31]

Relaxivity of Gd-Me_2DO2A encapsulated in apoferritin

A phantom image of the dextran-coated apoferritin that encapsulated Gd-Me_2DO2A (apoferritin MRI CA) is shown in Figure 4. Interestingly, the apoferritin encapsulating 11 Gd-Me_2DO2A molecules in the cavity shows a proton relaxivity of 35.9 $mmol^{-1}\cdot s^{-1}$ (on the basis of Gd concentration), which is 10-fold higher than that of Gd-DOTA. This high relaxivity should be attained by the immobilization of Gd-Me_2DO2A on the inner surface of apoferritin to increase the rotational correlation time (called the macromolecular effect), in addition to Gd-Me_2DO2A having more coordination sites for water than Gd-DOTA. With the increased number of the encapsulated Gd-Me_2DO2A molecules from 11 to 36, the proton relaxivity was decreased to about half.

Safety of the apoferritin-MRI CA

Gd-Me_2DO2A encapsulated in apoferritin was stored in a bovine blood serum solution at 4°C for one week to examine the stability. No Gd ions leaking from the apoferritin cavity were detected by ICP measurement, indicating that Gd-Me_2DO2A is stably located in apoferritin (Supplementary Figure S5). Even if the Gd complex was released from apoferritin and eliminated into the bloodstream, Gd-Me_2DO2A is considered to be smoothly discharged from the body via the kidney, and the released Gd shows no toxicity.

Acute toxicity of the apoferritin MRI CA was also preliminarily examined by a single-dose toxicity test. The apoferritin-MRI CAs were administered into the tail vein of 8-week-old nude mice (BALB/c nu/nu mice; SHIMIZU Laboratory Supplies Co. Ltd., Kyoto, Japan) at two different doses, where one dose was equal to that for an MR imaging experiment (group A, n = 4) and the other dose was 10-fold larger than group A's dosage (group B, n = 2). Body weight changes of these mice were traced for 2 weeks, and then autopsy diagnosis was performed. No mice in either group died during

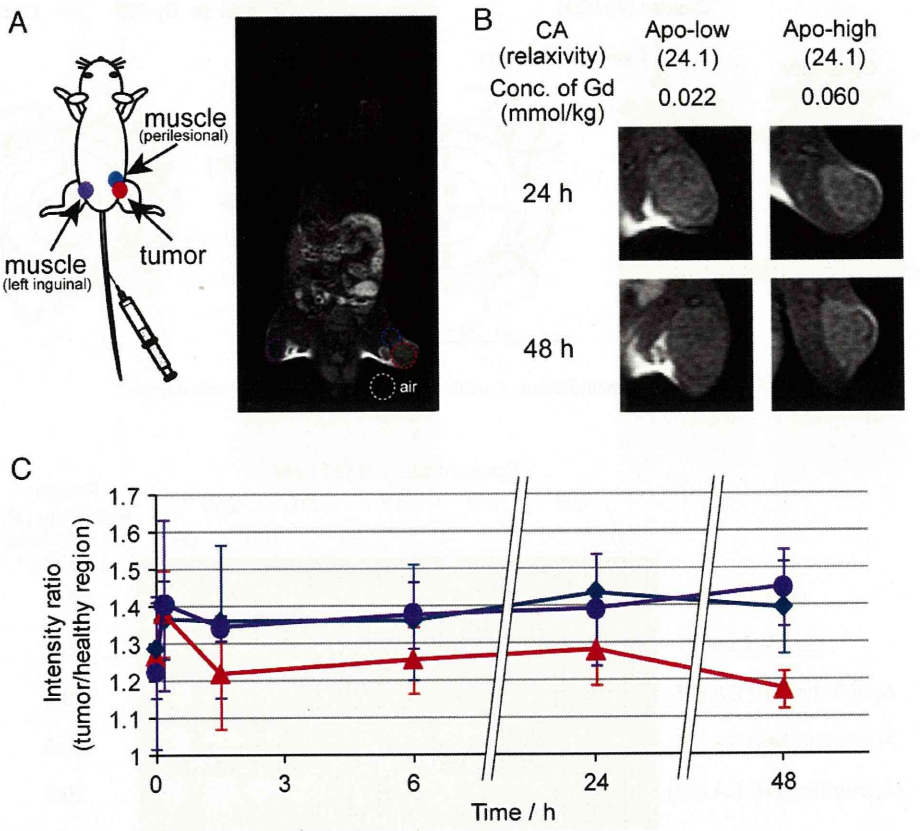

Figure 5. **(A)** Noncontrasted MR image of tumor-bearing mouse. **(B)** Magnitude MR images of the grafted tumor region using MRI CAs. **(C)** Time lapse image of brightness intensity ratio around tumor region (right inguinal region, red triangles) as compared to two healthy muscle regions of the left inguinal muscle (purple circles) and the perilesional region (blue diamonds). As CAs, apoferritin-encapsulated Gd-Me_2DO2A MRI CA: 0.022 mmol/kg (purple dots and blue diamonds), and Gd-DOTA: 0.13 mmol/kg (red triangles) were used.

the 2 weeks. The body weight of group B mice decreased during the first 2 or 3 days compared with that of reference groups, but no other serious side effects were observed. Toxicity tests will be reported in detail in another article.

MR imaging using tumor-bearing mouse

Apoferritin-MRI CA with relaxivity of 23.5 on a Gd basis was used for in vivo MR imaging. Its diameter as determined by dynamic light scattering measurement was 30 nm. Human cervical epithelial adenocarcinoma cells (HeLa) were subcutaneously transplanted into the right hind leg of immunodeficient nude mice. A buffered solution of the apoferritin-MRI CA was intravenously injected into the tumor-bearing mice, and T_1-weighted MR images were taken by the Toshiba EXCELART Vantage MRI system (1.5T, T_R = 500 ms, T_E = 15 ms). As a reference CA, the commercially available Gd-DOTA (Magnescope syringe; supplied by Guerbet Japan KK, Tokyo, Japan) was used. The amount of injected Gd-DOTA was decided based on the necessary quantity for human imaging (0.13 mmol/kg). Proton relaxivity of the apoferritin is about sixfold higher than that of Gd-DOTA. Therefore, concentration of the administered Gd of the apoferritin MRI CA was set to be 0.022 mmol/kg to adjust the CA net effects.

Figure 5, *A* and *B* show MR images of tumor-bearing mice with or without administration of apoferritin with Gd-Me_2-DO2A. The tumor region was imaged brighter than the healthy region (left inguinal muscle) and the perilesional muscle. With help of the CA, the contrast at the tumor region became more vivid. Figure 5, *C* shows time-dependent changes of the intensity ratios of the tumor region (right inguinal region) as compared to two healthy muscle regions of the left inguinal muscle and the perilesional region. Soon after the administration of the CA (10 minutes), the intensity ratios increased about 20%. In 24 hours, the intensity ratio showed the highest value (1.45) and remained relatively high even after 2 days. On the other hand, Gd-DOTA showed a similar intensity ratio increasing in the initial 10 minutes, but soon decreasing to the original level (red triangles). Gd-DOTA was rapidly cleared from the blood circulation through the kidneys. By using the Gd-Me_2DO2A encapsulated in apoferritin, the total amount of Gd ion for imaging was successfully reduced to 17% of Gd-DOTA with the same contrast effect in the tumor image, and the contrast can be retained for a prolonged period. When apoferritin-MRI CA was used at a higher concentration of 0.060 mmol/kg, which is about half of that in the case of the Gd-DOTA on a Gd concentration basis, the tumor region was imaged more clearly, as shown in Figure 5, *B* (Apo-high).

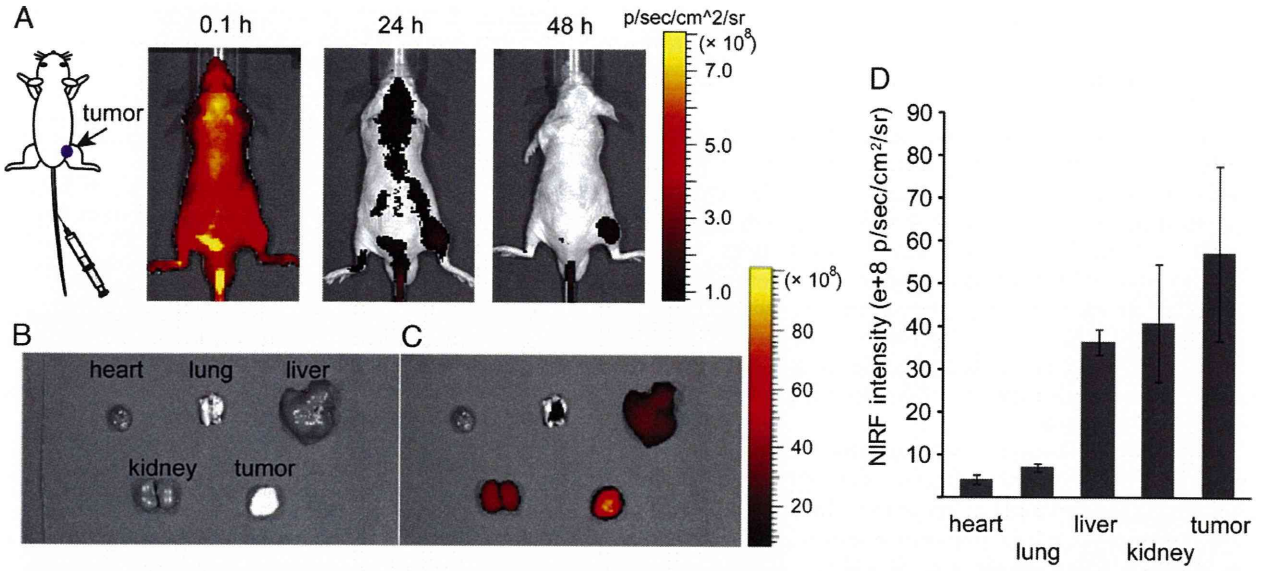

Figure 6. NIRF images of tumor-bearing mice using Dy-776 labeled apoferritin MRI CA, whose surface was coated with dextran. **(A)** Time lapse in vivo cancer imaging. **(B, C)** Ex vivo optical and NIRF images of isolated five organs after 48 hours from administration. **(D)** NIRF intensities of isolated organs.

To confirm that the apoferritin was responsible for the specific accumulation of Gd in the tumor xenograft, the disposition of the apoferritin itself was examined by NIRF image using Dy-776 (Dyomics), which was introduced onto the apoferritin outer surface (Figure 6, *A*). Soon after the administration (0.1 hour), the apoferritin-MRI CA was widely spread in the entire body of the mouse. With time, the excess amount of the apoferritin was excreted from the body, and NIRF signal intensity in normal tissues was decreased. On the other hand, NIRF signal obviously remained at the tumor region. Tumor was clearly imaged by NIRF 24 hours after administration, indicating that apoferritin coated with dextran should accumulate in the tumor region by the EPR effect. Figure 6, *B* and *C* show ex vivo NIRF images of several organs at 48 hours after administration. The strongest fluorescence signal was observed at the tumor region compared with others including liver (Figure 6, *C*). Although the NIRF signal intensity is not strictly quantitative, integrated NIRF signal intensity from tumor was the strongest among five isolated organs and reached 1.5 times higher than that from liver (Figure 6, *D*). NIRF and MR signals were detected at the same tumor region, confirming that Gd-Me_2DO2A is stably encapsulated in the apoferritin cavity in vivo.

Discussion

In this study we developed a new method of encapsulating small molecules into the apoferritin cavity utilizing electrostatic interaction, and prepared a new high-contrast MRI CA. The high proton relaxivity attained was due to (1) an increased water coordination number from Gd-DOTA of 1 to Gd-Me_2DO2A of 3 per Gd ion, and (2) immobilization of Gd-Me_2DO2A on the inner surface of apoferritin to increase the rotational correlation time, called the macromolecular effect.

Importantly, Gd-DOTA and Gd-HPDO3A were not successfully condensed in apoferritin by this newly developed method. This observation suggests that condensation of Gd-Me_2DO2A into the apoferritin cavity is due to the electrostatic interaction between cationic Gd-Me_2DO2A and the anionic apoferritin inner surface. The Gd-Me_2DO2A concentration in feed was lowered from 0.1 M in the case of the previous method to 1.2×10^{-4} to 2.4×10^{-3} M by using this new method. The lowering of concentration by two or three orders of magnitude on preparation had another significant effect–that of reducing nonspecific binding of Gd chelates on the apoferritin outer surface. When the Gd chelate concentration was high in the encapsulation process, a careful purification procedure (e.g., multiple purifications by size exclusion chromatography) was required to remove the excess Gd chelates. In the case where the feed ratio of Gd chelate to apoferritin was 10,000, the excess amount of Gd chelate could not be washed out by a single purification process using size exclusion chromatography, Sephacryl S-100 (data not shown). It is obvious that undesired adsorption of Gd-chelate onto the apoferritin outer surface is also decreased by lowing the Gd chelate concentration at the encapsulation process.

Increasing the number of encapsulated Gd-Me_2DO2A molecules from 11 to 36 resulted in a decrease of the proton relaxivity by about half. This result also supports the immobilization of Gd-Me_2DO2A on the apoferritin surface. The number of Gd-Me_2DO2A immobilization sites on the apoferritin inner surface is probably limited, and the excess Gd-Me_2DO2A may be weakly bound to the inner surface. Proton relaxivity of the weakly bound Gd-Me_2DO2A is not high. Therefore, proton relaxivity of averages would be decreased by virtue of the limited strong Gd-Me_2DO2A binding sites on the apoferritin inner surface.

Considering the proton relaxivity on an apoferritin concentration basis, the proton relaxivity of apoferritin encapsulating 36 molecules of Gd-Me_2DO2A was over 700 $mmol^{-1} \cdot s^{-1}$. Proton

relaxivity of apoferritin encapsulating 10 Gd-HPDO3A was reported to be 80 $mmol^{-1} \cdot s^{-1}$ on a Gd concentration basis.[16] Therefore, apoferritin-based proton relaxivities are almost the same level between these two cases.

However, we considered that our apoferritin MRI CA is preferable to apoferritin encapsulating Gd-HPDO3A for the following reasons. The expected proton relaxivity, which is increased by the macromolecular effect, is normally up to 30 $mmol^{-1} \cdot s^{-1}$ refs. [32-35]. A proton relaxivity of 80 $mmol^{-1} \cdot s^{-1}$ is high in view of the general consideration. Moreover, Gd-HPDO3A is an electrically neutral chelate and shows no electrostatic interaction with apoferritin. The high relaxivity might be explained by Gd chelate nonspecific adsorption on the apoferritin surface due to the high Gd chelate concentration in the encapsulation process.

A cationic Gd chelate, which has three water coordination sites and shows twofold higher proton relaxivity than Gd-DOTA, is efficiently encapsulated in apoferritin. The Gd chelates are bound to the inner surface of apoferritin to increase the relaxivity in total of 10-fold higher than Gd-DOTA. Decorating the apoferritin surface with dextran leads to accumulation of the apoferritin-MRI CA in the transplanted tumor region due to the EPR effect. The required amount of Gd for tumor imaging is successfully reduced by the high proton relaxivity of the apoferritin-MRI CA. Chemical design of the chelator and the chemical modification of the nanocage demonstrated here should be useful for development of the coming MR imaging CA.

Appendix A. Supplementary data

Supplementary data associated with this article can be found, in the online version, at doi:10.1016/j.nano.2011.01.015.

References

1. Caravan P, Ellison JJ, McMurry TJ, Lauffer RB. Gadolinium(III) chelates as MRI contrast agents: structure, dynamics, and applications. Chem Rev 1999;99:2293-352.
2. Corot C, Robert P, Idee JM, Port M. Recent advances in iron oxide nanocrystal technology for medical imaging. Adv Drug Deliv Rev 2006;58:1471-504.
3. Nainani N, Panesar M. Nephrogenic systemic fibrosis. Am J Nephrol 2009;29:1-9.
4. Cacheris WP, Quay SC, Rocklage SM. The relationship between thermodynamics and the toxicity of gadolinium complexes. Magn Reson Imaging 1990;8:467-81.
5. Ogata T, Terakado Y. Rare earth element abundances in some seawaters and related river waters from the Osaka Bay area, Japan: significance of anthropogenic Gd. Geochem J 2006;40:463-74.
6. Makino A, Kizaka-Kondoh S, Yamahara R, Hara I, Kanzaki T, Ozeki E, et al. Near-infrared fluorescence tumor imaging using nanocarrier composed of poly(L-lactic acid)-*block*-poly(sarcosine) amphiphilic polydepsipeptide. Biomaterials 2009;30:5156-60.
7. Tanisaka H, Kizaka-Kondoh S, Makino A, Tanaka S, Hiraoka M, Kimura S. Near-infrared fluorescent labeled peptosome for application to cancer imaging. Bioconjug Chem 2008;19:109-17.
8. Lukyanov AN, Hartner WC, Torchilin VP. Increased accumulation of PEG-PE micelles in the area of experimental myocardial infarction in rabbits. J Control Release 2004;94:187-93.
9. Hashizume H, Baluk P, Morikawa S, McLean JW, Thurston G, Roberge S, et al. Openings between defective endothelial cells explain tumor vessel leakiness. Am J Pathol 2000;156:1363-80.
10. Monsky WL, Fukumura D, Gohongi T, Ancukiewcz M, Weich HA, Torchilin VP, et al. Augmentation of transvascular transport of macromolecules and nanoparticles in tumors using vascular endothelial growth factor. Cancer Res 1999;59:4129-35.
11. Toussaint L, Bertrand L, Hue L, Crichton RR, Declercq JP. High-resolution x-ray structures of human apoferritin H-chain mutants correlated with their activity and metal-binding sites. J Mol Biol 2007;365:440-52.
12. Liu XF, Theil EC. Ferritins: dynamic management of biological iron and oxygen chemistry. Accounts Chem Res 2005;38:167-75.
13. Trikha J, Theil EC, Allewell NM. High-resolution crystal-structures of amphibian red-cell L-ferritin–potential roles for structural plasticity and solvation in function. J Mol Biol 1995;248:949-67.
14. Harrison PM, Arosio P. Ferritins: molecular properties, iron storage function and cellular regulation. Biochim Biophys Acta 1996;1275: 161-203.
15. Ilari A, Stefanini S, Chiancone E, Tsernoglou D. The dodecameric ferritin from *Listeria innocua* contains a novel intersubunit iron-binding site. Nat Struct Biol 2000;7:38-43.
16. Aime S, Frullano L, Crich SG. Compartmentalization of a gadolinium complex in the apoferritin cavity: a route to obtain high relaxivity contrast agents for magnetic resonance imaging. Angew Chem Int Edn 2002;41:1017-9.
17. Douglas T, Ripoll DR. Calculated electrostatic gradients in recombinant human H-chain ferritin. Protein Sci 1998;7:1083-91.
18. Kumar K, Chang CA, Francesconi LC, Dischino DD, Malley MF, Gougoutas JZ, et al. Synthesis, stability, and structure of gadolinium(III) and yttrium(III) macrocyclic poly(amino carboxylates). Inorg Chem 1994;33:3567-75.
19. Cacheris WP, Nickle SK, Sherry AD. Thermodynamic study of lanthanide complexes of 1,4,7-triazacyclononane-*N,N',N''*-triacetic acid and 1,4,7,10-tetraazacyclododecane-*N,N',N'',N'''*-tetraacetic acid. Inorg Chem 1987;26:958-60.
20. Lin SP, Brown JJ. MR contrast agents: physical and pharmacologic basics. J Magn Reson Imaging 2007;25:884-99.
21. Chang CA, Chen YH, Chen HY, Shieh FK. Capillary electrophoresis, potentiometric and laser excited luminescence studies of lanthanide(III) complexes of 1,7-dicarboxymethyl-1,4,7,10-tetraazacyclododecane (DO2A). J Chem Soc Dalton Trans 1998;19:3243-8.
22. Huskens J, Torres DA, Kovacs Z, Andre JP, Geraldes C, Sherry AD. Alkaline earth metal and lanthanide(III) complexes of ligands based upon 1,4,7,10-tetraazacyclododecane-1,7-bis(acetic acid). Inorg Chem 1997;36:1495-503.
23. Yang XK, Chasteen ND. Molecular diffusion into horse spleen ferritin: a nitroxide radical spin probe study. Biophys J 1996;71:1587-95.
24. Yang DW, Nagayama K. Permeation of small molecules into the cavity of ferritin as revealed by proton nuclear-magnetic-resonance relaxation. Biochem J 1995;307:253-6.
25. Simsek E, Kilic MA. Magic ferritin: a novel chemotherapeutic encapsulation bullet. J Magn Magn Mater 2005;293:509-13.
26. Webb B, Frame J, Zhao Z, Lee ML, Watt GD. Molecular entrapment of small molecules within the interior of horse spleen ferritin. Arch Biochem Biophys 1994;309:178-83.
27. Lowry OH, Rosebrough NJ, Farr AL, Randall RJ. Protein measurement with the folin phenol reagent. J Biol Chem 1951;193:265-75.
28. Stefanini S, Cavallo S, Wang CQ, Tataseo P, Vecchini P, Giartosio A, et al. Thermal stability of horse spleen apoferritin and human recombinant H apoferritin. Arch Biochem Biophys 1996;325:58-64.
29. Axen R, Ernback S. Chemical fixation of enzymes to cyanogen halide activated polysaccharide carriers. Eur J Biochem 1971;18: 351-60.
30. Passirani C, Barratt G, Devissaguet JP, Labarre D. Long-circulating nanoparticles bearing heparin or dextran covalently bound to poly (methyl methacrylate). Pharm Res 1998;15:1046-50.

31. Wang M, Thanou M. Targeting nanoparticles to cancer. Pharmacol Res 2010;62:90-9.
32. Aime S, Gianolio E, Uggeri F, Tagliapietra S, Barge A, Cravotto G. New paramagnetic supramolecular adducts for MRI applications based on non-covalent interactions between Gd(III)-complexes and beta- or gamma-cyclodextrin units anchored to chitosan. J Inorg Biochem 2006; 100:931-8.
33. Mohs AM, Zong YD, Guo JY, Parker DL, Lu ZR. PEG-*g*-poly (GdDTPA-*co*-L-cystine): effect of PEG chain length on in vivo contrast enhancement in MRI. Biomacromolecules 2005;6:2305-11.
34. Aime S, Chiaussa M, Digilio G, Gianolio E, Terreno E. Contrast agents for magnetic resonance angiographic applications: H-1 and O-17 NMR relaxometric investigations on two gadolinium(III) DTPA-like chelates endowed with high binding affinity to human serum albumin. J Biol Inorg Chem 1999;4:766-74.
35. Rebizak R, Schaefer M, Dellacherie E. Polymeric conjugates of Gd^{3+}-diethylenetriaminepentaacetic acid and dextran. 2. influence of spacer arm length and conjugate molecular mass on the paramagnetic properties and some biological parameters. Bioconjug Chem 1998;9: 94-9.

A Pre-targeting Strategy for MR Imaging of Functional Molecules Using Dendritic Gd-Based Contrast Agents

Kohei Sano, Takashi Temma, Takashi Azuma, Ryusuke Nakai, Michiko Narazaki, Yuji Kuge & Hideo Saji

Molecular Imaging and Biology

ISSN 1536-1632
Volume 13
Number 6

Mol Imaging Biol (2011) 13:1196-1203
DOI 10.1007/s11307-010-0463-1

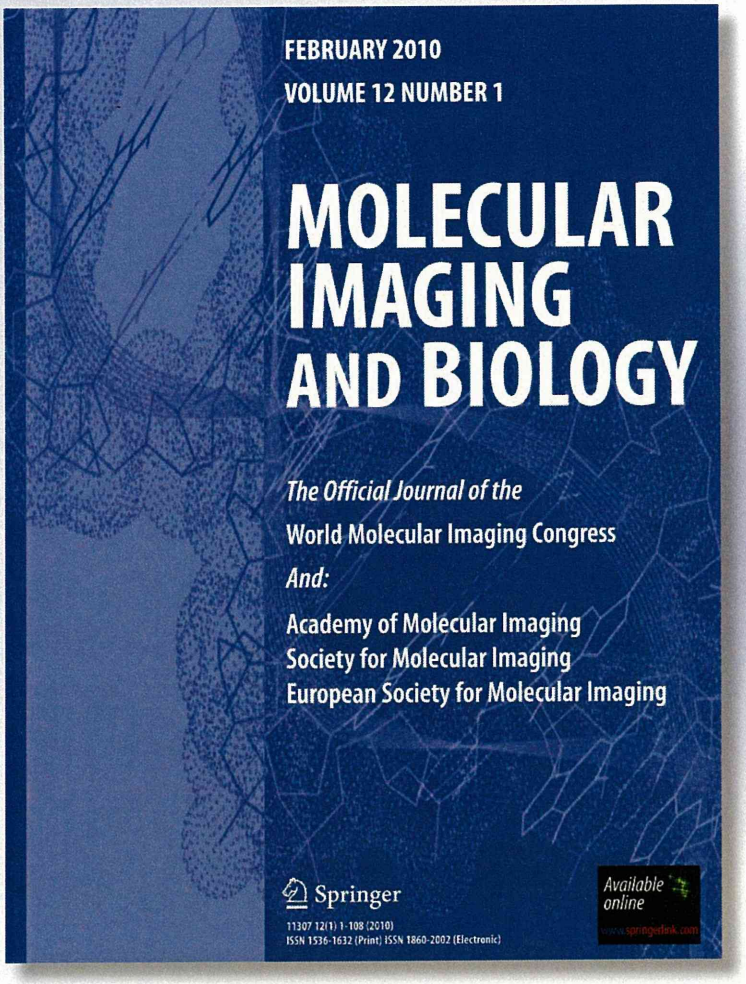

Springer

MOLECULAR IMAGING AND BIOLOGY

Published Online: 8 December 2010

Mol Imaging Biol (2011) 13:1196–1203
DOI: 10.1007/s11307-010-0463-1

RESEARCH ARTICLE

A Pre-targeting Strategy for MR Imaging of Functional Molecules Using Dendritic Gd-Based Contrast Agents

Kohei Sano,[1] Takashi Temma,[1] Takashi Azuma,[2] Ryusuke Nakai,[2] Michiko Narazaki,[3] Yuji Kuge,[1,4] Hideo Saji[1]

[1]*Department of Patho-Functional Bioanalysis, Graduate School of Pharmaceutical Sciences, Kyoto University, 46-29 Yoshida Shimoadachi-cho, Sakyo-ku, Kyoto, 606-8501, Japan*
[2]*Department of Medical Simulation Engineering Research Center for Nano Medical Engineering Institute for Frontier Medical Sciences, Kyoto University, Kyoto, 606-8501, Japan*
[3]*Department of Systems Science, Graduate School of Informatics, Kyoto University, Kyoto, 606-8501, Japan*
[4]*Central Institute of Isotope Science, Hokkaido University, Sapporo, 060-8638, Japan*

Abstract

Purpose: We aimed to establish a magnetic resonance imaging (MRI) protocol for the sensitive and specific imaging of functional molecules with a pre-targeting strategy utilizing the streptavidin–biotin interaction. Membrane type-1 matrix metalloproteinase (MT1-MMP) was selected as the target molecule.

Procedures: The biotinylated polyamidoamine dendrimer (PAMAM)-based contrast agent (Bt-PAMAM-DTPA(Gd)) was prepared, and its proton relaxivity ($r1$) and affinity to streptavidin were evaluated. Tumor-bearing mice were pre-targeted with streptavidin-conjugated anti-MT1-MMP monoclonal antibody (mAb), streptavidin-conjugated negative control IgG, or saline and 3 days later were injected with Bt-PAMAM-DTPA(Gd) followed immediately by MRI for a period of 3 h.

Results: High $r1$ (15.5 L $mmol^{-1}$ s^{-1}) and 1.9-fold higher affinity than D-biotin were obtained. Significantly higher relative tumor signals were observed in mice pre-targeted with streptavidin-conjugated anti-MT1-MMP mAb (165% at 3 h *vs.* pre-administration) than with saline or streptavidin-conjugated negative control IgG ($P<0.0001$).

Conclusions: This pre-targeting approach can accomplish sensitive and specific *in vivo* MRI of functional molecules.

Key words: Pre-targeting, Polyamidoamine dendrimer (PAMAM), Membrane type-1 matrix metalloproteinase, Magnetic resonance imaging

Introduction

Magnetic resonance imaging (MRI), characterized by a remarkable spatial resolution, is a powerful tool for noninvasive morphologic diagnosis of diseases including cancer. Recently, the application of MRI to functional molecular imaging coupled with anatomical information has been explored. To realize functional molecular imaging by MRI, contrast agents are required that possess a high relaxation to produce high MR signals to compensate for the low intrinsic sensitivity of MRI [1] in addition to selectively accumulating in the targeting site.

Gadolinium (Gd) chelates conjugated to macromolecules such as liposomes, micelles, and dendrimers can give rise to enhanced proton relaxivities in comparison with simple,

Correspondence to: Hideo Saji; *e-mail:* hsaji@pharm.kyoto-u.ac.jp

small molecule contrast agents such as Gd-diethylenetriamine pentaacetic acid (Gd-DTPA) [2–4]. This effect is due to a restriction in thermal flexibility leading to increased interactions between the Gd atom and surrounding water molecules [5–7]. Some groups have developed monoclonal antibody (mAb)-conjugated macromolecular contrast agents for imaging integrin αvβ3 or human epidermal growth factor receptor type 2 (HER2) in tumors, which successfully increased the tumor signal intensity by 15–30% [8, 9]. However, many researchers have failed to demonstrate *in vivo* functional molecular imaging using macromolecules conjugated with several Gd chelates and targeting moieties like antibodies and peptides because the pharmacokinetics of the targeting moieties was significantly altered by the introduction of macromolecular contrast agents, which resulted in low target recognition and high accumulation of the labeling agent in non-targeted tissues [10, 11]. Furthermore, when antibody-conjugated macromolecular contrast agents are injected at a Gd dose (0.1 mmol Gd/kg) necessary for adequate imaging, excess antibodies (on the order of milligrams per mouse) are typically administered, which leads to major limitations of cost and *in vivo* toxicity.

Thus, in this study, to overcome these problems and to realize functional molecular MRI by a macromolecule-based contrast agent, we aimed to use a pre-targeting strategy that utilizes the high affinity interaction between streptavidin and biotin ($Kd=10^{-15}$ M) [12]. In this pre-targeting method, the first step is to administer a streptavidin-conjugated target-specific antibody. In the second step, after selective accumulation of streptavidin-conjugated antibody in the targeted tissue and clearance of unbound targeting agent from the circulation, a biotin-bound imaging probe is injected. As the post-administration contrast agent, polyamidoamine dendrimer (PAMAM) was selected as the base structure since it is structurally well-defined and functional moieties including biotins and Gd chelates for both targeting and signal emission functions can easily be attached to the large number of its surface amino groups. The pre-targeting strategy is expected to provide selective and effective accumulation of the PAMAM-based contrast agent to the targeted site and a high S/N ratio during the first hours following administration, as has been observed in radioimmunotherapy and radioimmunodetection [13–16], and to potentially lead to lower *in vivo* toxicity [17, 18].

Thus, in this paper, we describe our efforts to establish a sensitive and specific *in vivo* MRI protocol for imaging functional molecules utilizing a pre-targeting strategy that combines a streptavidin-conjugated antibody with a PAMAM-based contrast agent modified with biotins. As the targeted biomolecule, membrane type-1 matrix metalloproteinase (MT1-MMP) was selected. Since MT1-MMP is exclusively expressed in tumors and is closely associated with metastasis [19] and invasion [20], MT1-MMP is a potential imaging target for evaluating tumor malignancy.

Materials and Methods

Synthesis of Streptavidin-Conjugated Anti-MT1-MMP mAb

Streptavidin-conjugated anti-MT1-MMP mAb and streptavidin-conjugated negative control IgG were synthesized according to a previously described method [14]. Briefly, EZ-Link® sulfosuccinimidyl-6-(biotinamido) hexanoate (sulfo-NHS-LC-biotin; Pierce, Inc.) was added to a solution of anti-MT1-MMP mAb (113-5B7, Daiichi Fine Chemical Co.) in a molar ratio of 12:1. The mixture was gently stirred for 30 min at room temperature and then was purified with a diafiltration membrane (Amicon Ultra 4 (MWCO 30,000), Millipore Co.). A solution of biotinylated anti-MT1-MMP mAb was added to a solution of streptavidin (SAv; Pierce, Inc.) in a 1:3 molar ratio. The mixture was incubated for 1 h at 37°C followed by purification twice by affinity chromatography using a HiTrap rProtein A column (GE Healthcare Bioscience). The eluate containing anti-MT1-MMP mAb-SAv was concentrated with a diafiltration membrane (MWCO 30,000), and the protein concentration was determined by the bicinchoninate (BCA) method. The purification was monitored by a size exclusion chromatograph using a 300×4.6-mm i.d. TSK-Gel Super SW 3000 column (Tosoh Co., Japan) eluted with phosphate buffer (0.1 M, pH 6.8) at a flow rate of 0.1 mL/min. Comparison of molecular mass standards (Oriental Yeast Co., Japan) of the absorbance at 280 nm indicated that a peak at 30.3 min was consistent with the presence of a 210-kDa streptavidin-conjugated anti-MT1-MMP mAb. Furthermore, streptavidin-conjugated anti-MT1-MMP mAb retained 81.3% of the anti-MT1-MMP mAb immunoreactivity, which was confirmed by flow cytometry.

Synthesis of Bt-PAMAM-DTPA(Gd)

EZ-Link® sulfo-NHS-LC-biotin was added to a solution of PAMAM (generation 4 (G4)) (Sigma Aldrich) in a molar ratio of 20:1. The mixture was stirred for 30 min at room temperature and then was applied to a diafiltration membrane (MWCO 10,000) to remove unbound biotins as well as to change the buffer to phosphate buffer (0.1 M, pH 9.0). After purification, the incorporation ratio of biotins conjugated to each dendrimer was measured using an EZ™ Biotin Quantitation Kit (Pierce, Inc.). The biotinylated PAMAM was reacted with a 64-fold molar excess of 2-(*p*-isothiocyanatobenzyl)-diethylenetriamine pentaacetic acid (*p*-SCN-Bz-DTPA) (Macrocyclics) at 40°C for 24 h. During the reaction, the pH was maintained at 9.0 with 1 N NaOH. An additional equal amount of *p*-SCN-Bz-DTPA was added after 24 h, and the reaction was incubated for another 24 h at 40°C. The resulting preparation was purified by diafiltration membrane (MWCO 10,000). After purification, the number of DTPAs incorporated into each G4 dendrimer was checked by chelate titration using $ZnSO_4$ (indicator: 4-(2-pyridylazo)resorcinol, NH_3/NH_4^+, pH 10), according to a previously described method with some modification [21]. Purified Bt-PAMAM-DTPA was mixed with $GdCl_3$ (Sigma Aldrich) in citrate buffer (0.3 M, pH 5.0) for 2 h at 40°C. The excess Gd was removed by diafiltration membrane (MWCO 10,000) while simultaneously changing the buffer to PBS (0.1 M, pH 7.4). The number of Gd incorporated into the dendrimer was checked by separating the free Gd and Bt-PAMAM-DTPA

(Gd) with a diafiltration filter after labeling the Bt-PAMAM-DTPA with ^{153}Gd and nonradioactive Gd. For comparison purposes, PAMAM-DTPA(Gd) containing one biotin (Bt_1-PAMAM-DTPA (Gd)) was also prepared in a similar manner.

Stability of Bt-PAMAM-DTPA(Gd) in Mouse Plasma

^{153}Gd-labeled Bt-PAMAM-DTPA(Gd) was prepared by reacting Bt-PAMAM-DTPA(Gd) with ^{153}Gd (1 μCi, PerkinElmer Japan Co., Osaka, Japan) and non-radioactive Gd in 0.3 M citrate buffer at pH 5.0 for 2 h at 40°C. ^{153}Gd-labeled Bt-PAMAM-DTPA(Gd) (30 μL) was added to mouse plasma collected from female C3H/He mice (270 μL), and the plasma samples were incubated at 37°C for 0, 3, and 24 h. After incubation, aliquots of the samples were drawn, and radioactivity was analyzed by size-exclusion chromatography with a PD-10 column (GE Healthcare Bioscience) using saline as eluent.

Affinity of Bt-PAMAM-DTPA(Gd) for Streptavidin

Competition assays of ^{125}I-(3-iodobenzoyl)norbiotinamide (^{125}I-IBB), a radiolabeled biotin derivative synthesized as reported previously [22], were performed by incubating streptavidin (Pierce, Inc.; 400 μL, 2 μg/mL), ^{125}I-IBB (50 μL, 5 μCi), and various concentrations of Bt-PAMAM-DTPA(Gd), Bt_1-PAMAM-DTPA(Gd), and D-biotin (Nacalai Tesque, Kyoto, Japan; 50 μL, 10^{-8}~10^{-4} M) in PBS (0.1 M, pH 7.4) for 60 min at 37°C. At the end of the incubation, the mixture was applied to a size exclusion column with a Sephadex G-50 Fine (GE Healthcare Bioscience), followed by measurement of the radioactivity from the column eluent (containing macromolecules) with a NaI well-type scintillation counter (1470WIZARD, PerkinElmer Japan Co.). Nonspecific binding was determined in the presence of 10 mg/mL D-biotin. The 50% inhibitory concentrations (IC_{50}s) were determined from displacement curves of the percent inhibition of ^{125}I-IBB binding *vs.* the inhibitor concentration.

Preparation of Tumor-Bearing Animals

Female C3H/He mice (5 weeks old), supplied by Japan SLC Co. (Hamamatsu, Japan), were housed under a 12-h light/12-h dark cycle and were given free access to food and water. The animal experiments in this study were conducted in accordance with institutional guidelines and were approved by the Kyoto University Animal Care Committee, Japan.

FM3A mouse breast carcinoma cells were supplied by the Health Science Research Resources Bank (Osaka, Japan). They were cultured in DMEM medium (Nissui Pharmaceutical Co.) supplemented with 10% fetal bovine serum at 37°C in a humidified atmosphere containing 5% CO_2 and 95% air and had a 10.6-h doubling time.

FM3A cells were suspended in 0.01 M PBS (pH 7.4) followed by subcutaneous inoculation into the right hind leg of the mouse (5×10^6 cells/100 μL/mouse) [23]. The tumor volume was estimated by (length)×(width)^2/2 [24] over a 10-day tumor growth period. The average size of the tumors was 213±82 mm^3 on the MRI study day. The expression of MT1-MMP in FM3A cells and tumor tissues was confirmed by western blotting and immunohistochemistry [25].

Magnetic Resonance Imaging

MRI was performed using a clinical 1.5 Tesla MR scanner (MAGNETOM Symphony Sonata, Siemens). All T_1-weighted MR images were acquired with a multislice spin-echo pulse sequence. MRI data were analyzed using the ImageJ software.

Phantom Study

Solutions of Gd-DTPA (Sigma Aldrich) and Bt-PAMAM-DTPA (Gd) were prepared with a Gd concentration in the range of 10 to 500 μM in vials with an inner diameter of 15 mm followed by the MR scan using a knee coil (20.5 cm in diameter) at 20°C. To obtain proton relaxivity ($r1$) for samples, spin-echo images were obtained using a sequence with TR=500, 1,000, 1,500, and 2,000 ms and with TE=15 ms. The imaging parameters were as follows: field-of-view, 256×128 mm; matrix, 256×128; slice thickness, 7 mm; and number of average, 3.

In Vivo Study

Mice (n=4) bearing FM3A tumors in the right thigh received streptavidin-conjugated anti-MT1-MMP mAb (50 μg/100 μL in saline) via tail vein. Three days later, Bt-PAMAM-DTPA(Gd) (0.1 mmol Gd/kg, 100 μL in PBS (0.1 M, pH 7.4), i.v.) was injected followed by data acquisition by MRI at several time points over a 3-h post-injection period under sodium pentobarbital (50 mg/kg, i.p.) anesthesia. All MR images were obtained using a hand-made round surface coil (5.5 cm in diameter) fixed by a custom constructed coil holder. The imaging parameters were as follows: TR/TE, 300/5.2 ms; field-of-view, 128×96 mm; matrix, 256×192; slice thickness, 1.5 mm; and number of average, 3. MRI studies were also conducted as above on FM3A tumor-bearing mice (n=3) pre-treated with saline (100 μL) or streptavidin-conjugated negative control IgG (50 μg/100 μL in saline). The signal intensity was calculated by drawing a region of interest around the tumor, muscle in the contralateral hind limb, and kidneys. The relative signal intensity in each tissue was defined as the signal intensity after administration of Bt-PAMAM-DTPA(Gd) divided by the signal intensity before administration.

Statistical Analysis

Unpaired Student's t test was used to evaluate the significance of differences of $r1$ between Bt-PAMAM-DTPA(Gd) and Gd-DTPA. To compare the time courses of relative signal intensity in the tumor and kidneys and tumor/muscle (T/M) signal ratios among Bt-PAMAM-DTPA(Gd) pre-targeted by streptavidin-conjugated anti-MT1-MMP mAb, streptavidin-conjugated negative control IgG, and saline, two-way repeated measures ANOVA with post-hoc analysis by the Tukey–Kramer test was

performed. Differences at the 95% confidence level ($P<0.05$) were considered significant.

Results

Characterization of Bt-PAMAM-DTPA(Gd)

Bt-PAMAM-DTPA(Gd) was synthesized in four steps from PAMAM in a yield of 63%. PAMAM was conjugated to 9.9±1.3 biotins and 43.6±1.9 DTPAs, which were quantitatively coordinated to Gd. Bt_1-PAMAM-DTPA(Gd) containing 1.0±0.1 biotin and 47.6±2.2 DTPAs on PAMAM dendrimer was also synthesized. The ^{153}Gd-labeled Bt-PAMAM-DTPA(Gd), which was incubated with mouse plasma for 24 h, did not release any low molecular weight metabolites or free radiometals (Fig. 1).

The competitive binding assay revealed that all of the contrast agents inhibited the binding of ^{125}I-IBB to streptavidin in a dose-dependent manner (Fig. 2). The IC_{50}s for Bt-PAMAM-DTPA(Gd), Bt_1-PAMAM-DTPA(Gd), and D-biotin were 32±31, 1,390±1,220, and 60±45 nM, respectively, demonstrating that Bt-PAMAM-DTPA(Gd) had about 1.9- and 43.2-fold higher affinity to streptavidin than D-biotin and Bt_1-PAMAM-DTPA(Gd).

MR Imaging Study (Phantom Study)

The *in vitro* T_1-weighted MR images with Bt-PAMAM-DTPA(Gd) and Gd-DTPA are shown in Fig. 3a. Water and PBS were used as baselines. With the same Gd concentration, the signals with Bt-PAMAM-DTPA(Gd) were higher compared to Gd-DTPA. The longitudinal relaxation rate ($1/T_1$) *vs.* the concentration of Gd for both contrast agents are shown in Fig. 3b with good linear fits ($R^2=1.00$ and 0.99 for Bt-PAMAM-DTPA(Gd) and Gd-DTPA, respectively). Calculated $r1$ values (L mmol^{-1} s^{-1}) for Bt-PAMAM-DTPA(Gd) and Gd-DTPA were 15.5±1.1 and 3.6±0.1, respectively, which shows that the proton relaxivity of Bt-PAMAM-DTPA(Gd) was 4.3-fold higher than that of Gd-DTPA ($P<0.0001$).

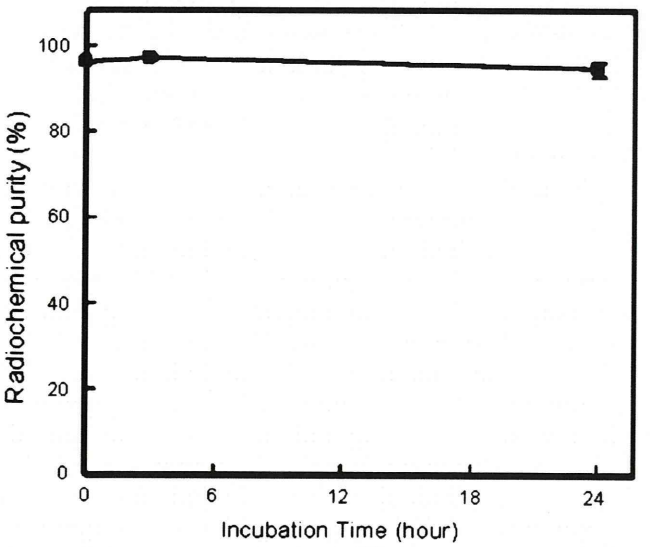

Fig. 1. Size exclusion analysis of ^{153}Gd-labeled Bt-PAMAM-DTPA(Gd) radioactivity after incubation at 37°C in mouse plasma. The *error bars* represent standard deviations.

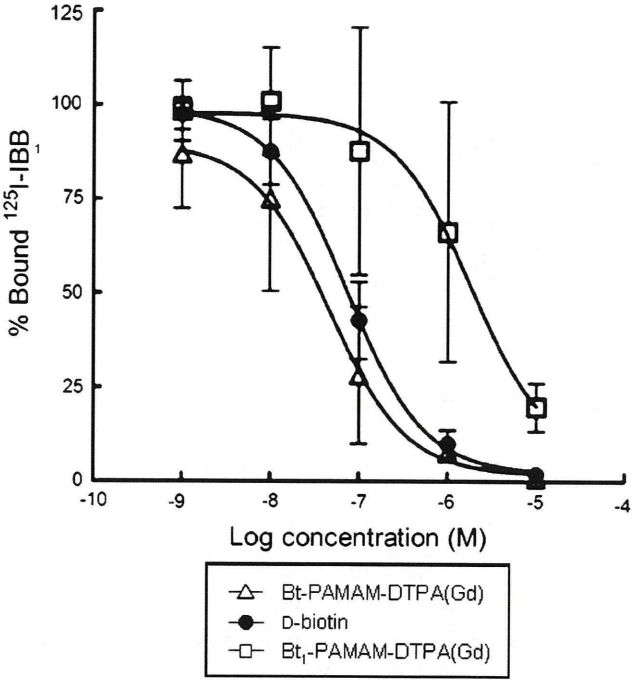

Fig. 2. Inhibition of ^{125}I-IBB binding to streptavidin by D-biotin, Bt-PAMAM-DTPA(Gd), or Bt_1-PAMAM-DTPA(Gd).

MR Imaging Study (In Vivo Study)

Fig. 4a (coronal) and b (transaxial) show *in vivo* T_1-weighted MR images of tumor-bearing mice before and at 5 and 180 min after injection of Bt-PAMAM-DTPA(Gd) following pre-treatment with streptavidin-conjugated anti-MT1-MMP mAb (MT1-MMP), streptavidin-conjugated negative control IgG (negative control), or saline (saline). In the MT1-MMP group, the most intense signal was observed in the margin of the tumor, as compared with the tumor core, over the 180-min period. The relative signal intensity (rSI) in the tumor and the relative T/M ratio were strongly enhanced just after administration of Bt-PAMAM-DTPA(Gd) and were highly maintained for 3 h after the contrast agent injection which displayed rapid clearance from the circulation (Fig. 4c, d). These signals were significantly greater than those from the negative control group ($P<0.05$ (at 44 and 55 min), $P<0.01$ (at 2 and 3 h)). In the saline group, Bt-PAMAM-DTPA(Gd) readily disappeared from the circulation and mainly accumulated in the kidneys. Though the relative signal intensity in the tumor also increased